Deltares

Enabling Delta Life

Sediment mapping of sand extraction pit Maasvlakte 2, using bed classification from multibeam backscatter data

Deltares

Sediment mapping of sand extraction pit Maasvlakte 2, using bed classification from multibeam backscatter data

dr Thaienne A.G.P. van Dijk
dr Marios Karaoulis
drs Timo C. Gaida
Rob J. van Galen
Saskia E. Huisman
Sieb de Vries
Edvard Ahlrichs

Deltares

Title

Sediment mapping of sand extraction pit Maasvlakte 2, using bed classification from multibeam backscatter data

Client	Project	Attribute	Pages
Rijkswaterstaat Zee en Delta, RIJSWIJK ZH	11202743-002	11202743-002-BGS-0002	51

Keywords

Sea-bed sediment mapping, bed classification, Bayesian method, multibeam backscatter, sand pit MV2

Summary

The distribution of sea bed sediments is relevant in understanding both physical processes and ecology in the marine environment. Modern and innovative techniques allow for high-resolution measurements for sediment mapping. In this project, we collected multibeam bathymetry and backscatter data, as well as box core samples for ground truthing, in and around the two sand extraction pits for Maasvlakte 2, offshore Rotterdam, Netherlands. We applied a Bayesian bed classification technique, as developed by Delft University of Technology, in order to create a high-resolution acoustic sediment classification map. This project is meant to be a pilot study, also aimed at knowledge exchange. Therefore, bed classification results are preliminary. The acoustic bed classification results in 4 acoustic classes. Assigning sediment characteristics, as derived from grain-size analyses of the box core samples, to the acoustic classes results in an acoustic sediment map. Differences in sediment characteristics in the study area are subtle, and yet the acoustic techniques are able to differentiate between these characteristics. The correlation of sediment characteristics to acoustic classes revealed that median grain size and mud content alone were not fully discriminative and that sediment sorting and gravel content correlated well to the acoustic classes. The influence of gravel content and other sediment and/or bed characteristics, such as thin mud drapes or benthic fauna, are discussed in this report. The absence of mud layers at the bed in 19 of 21 box core descriptions, grain-size analyses and 4 water samples suggest that the pit is not being filled in with mud at a significant rate. However, two fine-grained samples in the eastern part of the pit fall within an acoustic class that occurs in the eastern area that was first abandoned for dredging activities, which could imply that fine sediments are slowly accumulated. More rigorous interpretation of the method, resulting bed classification map and assignment of samples is required to fully understand the sedimentological conditions of these sand pits.

Deltares

Title
Sediment mapping of sand extraction pit Maasvlakte 2, using bed classification from multibeam backscatter data

Client	Project	Attribute	Pages
Rijkswaterstaat Zee en Delta, RIJSWIJK ZH	11202743-002	11202743-002-BGS-0002	51

References
11202743-000-BGS-0001 - Offerteaanvraag voor het project 'Multibeambackscatteropnamen zandwinput Maasvlakte 2'- zaaknummer 31144800.pdf
11202743-000-BGS-0002_v0.1-Offerte multibeam backscatter zandwinput MV2.pdf
11202743-000-BGS-0003 - Opdracht tot uitvoering project Multibeam backscatter zandwinput MV2 zaaknummer 31144800.pdf
11202743-002-BGS-0001 - van Dijk - RWS wvl - Uitstel van oplevering project Multibeam backscatter zandwinput MV2 zaaknummer 31144800.pdf
Contact at Rijkswaterstaat Ad Stolk

Version	Date	Authors	Initials	Review	Initials	Approval	Initials
0.1	sept. 2019	dr T.A.G.P. van Dijk	TvD	dr Mirjam Snellen (Delft University of Technology)	MS	drs M. Blauw	MB
		dr M. Karaoulis					
		T.C. Gaida					
		R.J. van Galen					
		S.E. Huisman					
		S. de Vries					
		E. Ahlrichs					

Status
final

Contents

1 Introduction

1.1 Aim and rationale

Rijkswaterstaat asked Deltares to map the seabed sediments of the sand extraction pits of Maasvlakte 2, using an innovative method of acoustic bed classification, developed by Delft University of Technology, based on multibeam echo sounder bathymetry and backscatter measurements and box coring. Data collection offshore is part of this research. The aim of this research is to establish the distribution of sand and mud in the pits. Since sediment composition is one of the most important factors for benthic fauna, it is crucial to map the distribution of sand and mud at high-resolution in order to evaluate human interventions in the creation and use of the (very) deep extraction pits in light of future, large-scaled sand extraction. The outcome of this investigation will be used in the assessment of the consequences of the construction of Maasvlakte 2.
The classical methodology of seabed mapping is based on bed sampling (cores or grab samples), which are then interpolated to an area-covering seabed sediment map. The great advantage of bed classification using multibeam backscatter is that the resulting map is a high-resolution map that is compiled from real measurements (as opposed to interpolation of low-density point data) in a very efficient and cost-effective way.

A secondary aim of this project is knowledge exchange and development through a collaboration among Delft University of Technology, Deltares and Rijkswaterstaat in the field of multibeam backscatter and acoustic bed classification. The interpretation of the bed classification in this project leads to the sedimentological characterisation of the Maasvlakte 2 extraction pits and the surrounding seabed. Deltares financially contributes towards this aim from the multiyear Strategic Research Programme “Subsurface resources in a circular economy”.

1.2 Theoretical background to multibeam (MBES) and MBES-backscatter

Acoustic waves are the most commonly used method to investigate the seabed and subsurface. The state of the art of the depth measurement equipment was evaluated by the working group on S-44 preparing the 4th Edition in 1998 (IHO, 1988) as follows:

*“**Single beam echo sounders** have reached a sub-decimeter accuracy in shallow water. The market offers a variety of equipment with different frequencies, pulse rates etc. and it is possible to satisfy most users' and, in particular, the hydrographers' needs. (…)*
***Multibeam echo sounder** technology is developing rapidly and offers great potential for accurate and total seafloor search if used with proper procedures and provided that the resolution of the system is adequate for proper detection of navigational hazards.”*

Multibeam echo sounders (MBESs) have become the most valuable tool for seafloor mapping providing high-resolution bathymetry and acoustic backscatter datasets [Lecours et al., 2016]. Various classification methods, employing MBES bathymetry, backscatter, and their second order moments, have been developed to characterize sea- or riverbeds in the last two decades [Brown et al., 2011]. These aim at maximizing the performance in discriminating between different seabed environments or sediment types. Acoustic backscatter strength is the most common feature used in seabed classification [Brown et al., 2011]. The backscatter strength is dependent on the composition of the seabed, angle of incidence, and acoustic frequency [Jackson & Richardson, 2007].

Basic concepts

The acoustic waves consist of subtle variations of the pressure field in the water column. Water particles move back and forth, in the direction of the propagation of the wave, producing adjacent regions of compression and expansion. Acoustic depth measurement systems measure the elapsed time that an acoustic pulse takes to travel from a generating transducer to the water bottom and back. This is illustrated in Figure 1 where the measured depth is between the transducer and some point on the acoustically reflective bottom. The travel time of the acoustic pulse depends on the sound speed (c) in the water column. If the sound speeds in the water column are known, along with the distance between the transducer and the reference water surface, the depth (d) can be computed by the measured travel time of the pulse.

Multibeam systems can also collect information about the type of seafloor. Different seafloor types "scatter" sound energy differently and hence return the signal with different levels of energy. This is known as backscatter, which is a property of the sediment. Therefore, backscatter information can be used to determine the physical nature of the bed and distinguish among seabed sediment types. For example, a softer bottom such as mud will return a weaker signal than a harder bottom, like rocks or gravel.

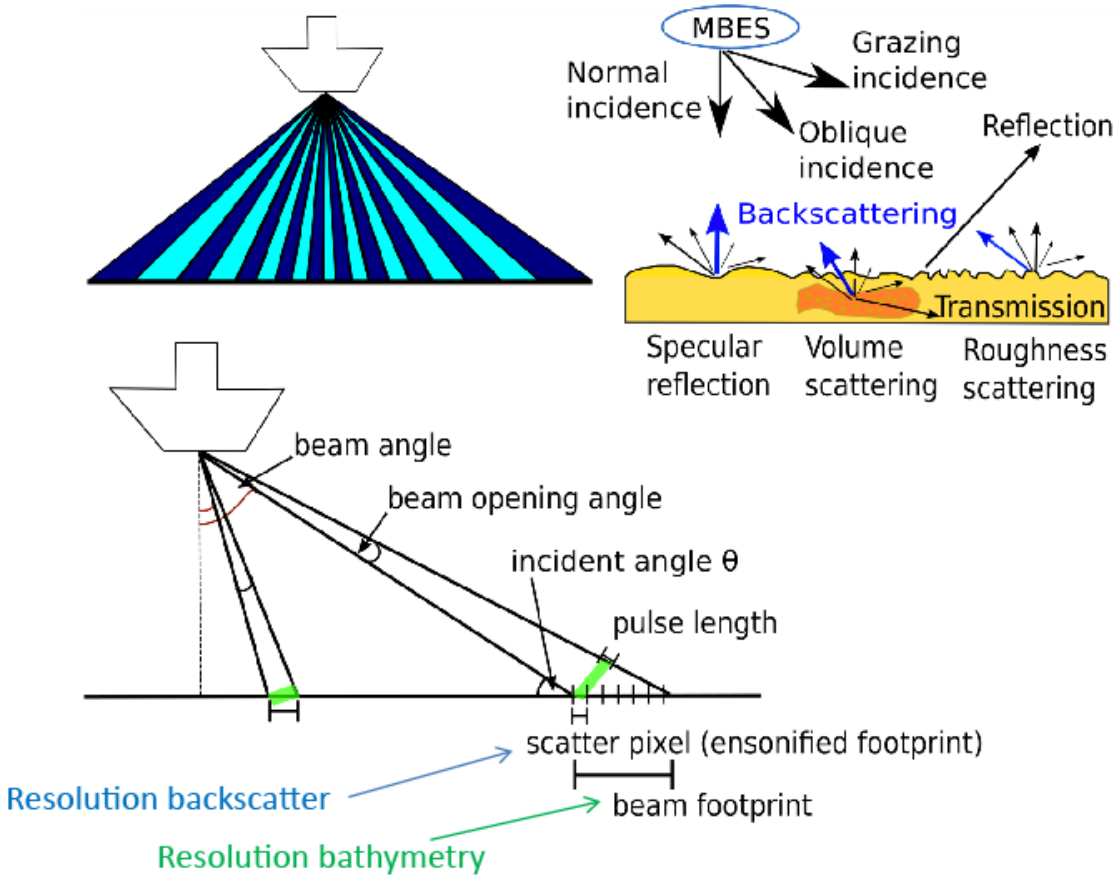

Figure 1: Terminology and basic principle of MBES-backscatter (Figure with courtesy of Timo C. Gaida).

The acquisition cycle starts with an emission from the sounder system. This action takes place in the emission unit, where the electric signal is transformed into an acoustic signal. In this process, a projector, such as a piezo-electric ceramic, is used. It is capable of producing a pressure wave with specific frequency characteristics when a voltage V is applied. The emitting signal is electronically steered into a narrow beam in the along-track direction of the vessel. The transmitted signal with a predefined source level, measured as SL, is attenuated due to sound absorption, scattering and energy spread along the travel path in the water column. These losses of energy are called transmission loss TL.

When the signal reaches the seafloor, it ensonifies an area of seafloor. In this area, the signal is reflected, refracted and scattered and only a small part of energy is scattered back towards the transducer in the arrival direction (backscattering). The amount of backscattered energy depends on the seabed properties, (e.g. roughness, density, volume heterogeneity), incident angle and frequency of the acoustic waves. The proportion normalized per unit area between the backscattered energy and the incident energy is called the backscatter strength, BS, of the seafloor (Figure 1).
While the backscattered signal travels back to the transducer, it suffers sound attenuation again. The acoustic signal level, EL, received at the transducer, can be expressed via the sonar equation [Nguyen et al., 2017; Gaida et al., 2018b] as follows:

$$BS_f(\varphi) = EL - SL - BP_T(f, \theta_T) + TL - PG - SH(f) - BP_R(f, \theta_R) - 10\log(A) \quad (1)$$

where SL is the source level (in dB re 1 µPa at 1 m), modulated by the transmission directivity pattern BP_T as a function of frequency, f, and the transmission angle θ_T with respect to the sonar axis. PG (in dB) is the receiver gain applied by the receiver electronics, SH (in dB re 1 V/µPa) is the transducer sensitivity with respect to f, and BP_R is the directivity pattern at reception expressed as a function of f and the receiving angle θ_R with respect to the sonar axis. BS_f is defined per m^2 and derived from the target strength $TS = BS_f + 10\log(A)$ (in dB re 1 m^2) via the ensonified footprint area A. The transmission loss TL depends on the water conditions and the travel distance R of the signal to the seabed. It can be written as

$$TL = 2\alpha R + 40\log(R) \quad (2)$$

where α (in dB/m) is the absorption coefficient depending on temperature, salinity, acidity, pressure, and f. The second term in Equation (2) accounts for the energy loss of the signal due to geometrical spreading. A is affected not only by the sonar characteristics but also by the seabed morphology, i.e., the across-track slope e_y and along-track slope e_x (radians). The ensonified footprint area in the pulse-limited regime A_p and in the beam-limited regime A_b, respectively, are expressed by [Amiri-Simkoei et al., 2009]

$$Ap = \Omega_{tx} R \, c\tau_{eff} / (2 \sin(\varphi_{fl} - e_y) \cos(e_x)) \quad (3)$$

and

$$A_b = R^2 \Omega_{tx} \Omega_{rx} \quad (4)$$

where c is the sound speed in water, τ_{eff} is the effective pulse length, and φ_{fl} is the incident angle with respect to nadir and a flat seabed. Ω_{tx} and Ω_{rx} are the beam opening angles (representing the −3 dB width of the main lobe) for transmission and reception and can be approximated for a continuous line array with length L and equally spaced transducer elements by [Lurton et al., 2010]

$$\Omega(\theta R,T) = \lambda/L \quad 1/\cos(\theta_{R,T}) \tag{5}$$

where λ is the wavelength of the transmitted signal given by λ = c/ f. The term 1/ cos($\theta_{R,T}$) in Equation (5) describes the increase of the beam opening angle with increasing steering angle θ due to the reduced projected line array length. Considering a constant array length, the beam width changes with varying frequency. Furthermore, to correct for seabed morphology, the incident angle with respect to the actual seabed φ is calculated from φ_{fl} (degrees) according to [Amiri-Simkoei et al., 2009]

$$\cos(\varphi) = \sin(90 - \varphi_{fl}) + \cos(90 - \varphi fl)e_y / (\text{sqrt}(1 + e^2_x + e^2_y)). \tag{6}$$

The incident angle correction assigns to each backscatter measurement the true incident angle. In environments with a rough seabed morphology (i.e. variations in bed slope angle), this correction is essential for seabed classification using backscatter data and was applied in this study (see Chapter 2). The sonar equation (Equation (1)) allows for the theoretical extraction of the absolute backscatter strength from the received signal of the MBES. However, the necessary variables and parameters might be neither available from the sonar producer nor measured sufficiently accurately. Even though all variables are properly documented, the conversion from analog to digital data and *vice versa* at reception and transmission often exhibits a discrepancy between the design and actual hardware implementation. In addition, aging of the MBES components might change the sensitivity of the system hardware over time [Schimel et al., 2018]. In such a case frequently performed relative or absolute calibrations of the MBES systems using natural reference areas or a calibrated single-beam echo sounder can be conducted [Roche et al., 2008; Eleftherakis et al., 2018]. If no calibration is performed, the backscatter data is considered as uncalibrated data (see Chapter 2 for calibration in this study). Still, as long as the relative variation of backscatter strength with respect to varying sediment types and incident angles are preserved within the processing, seabed classification (see section 2.4.2) can be applied, as conducted for the study area.

1.3 Study area

The study area comprises the two sand extraction pits for the construction of the Maasvlakte 2 (from hereon MV2), the most recent seaward extension of the Port of Rotterdam. The extraction pits are located approximately 15 km offshore the main Dutch coast (or 10 km offshore from MV2). The northern pit is located immediately south of the bend in the approach channel to the Port of Rotterdam (Figure 2).

The northern pit (North pit, or N-pit) is the main extraction pit, with a size of roughly 6 x 2 km and reaches down to a depth of 47.5 m -LAT, which is more than 20 m below the surrounding seabed (at water depths between 18.7 and 27 m -LAT). In the north-east part of this pit, dredging depth was limited, in order to spare the coarse-grained sediments, which are more valuable for industrial purposes, such as concrete and building, than elevating the Maasvlakte 2. In the dredging process, slopes were maintained at a slope ration of 1:7 to 1:10, in order to

prevent oxygen-deprivation of water in the pit. Dredging activities in the North-pit proceeded from east to west, whereby the eastern parts of the pit were abandoned first, since 2009/2010 (pers. comm. Ad Stolk, RWS, Dec 2018). The western part of the North-pit is still being dredged; the other parts of the North-pit are at maximum depth and are being ecologically monitored for recolonisation of macrobenthos (the report will be made available by RWS after this backscatter study). The southern pit is smaller, with a size of approximately 1.6 by 1.2 km, and although shallower than the northern pit, it reaches down to 38 m below LAT. Although the South-pit may still be excavated, in practice, there is little activity in this pit (pers. comm. Ad Stolk, RWS, Dec 2018).

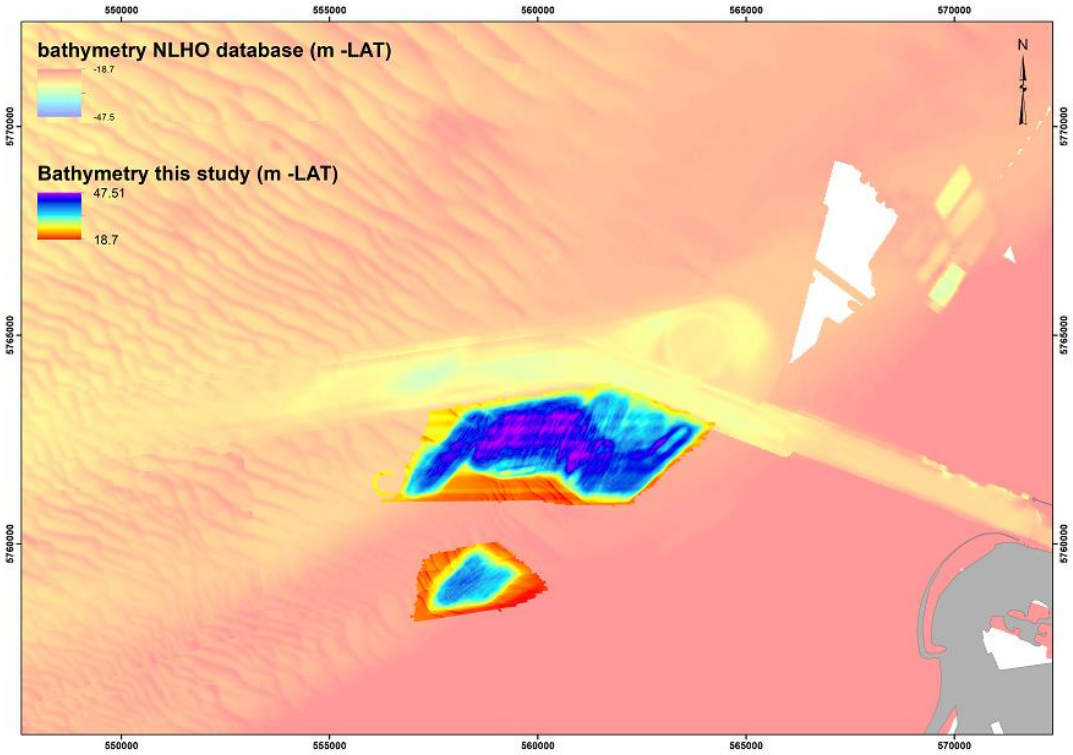

Figure 2: Bathymetric map of the study area (bright colours), with the larger-scaled bathymetry from the Hydrographic Office database in the background (faint colours). The map exhibits the location of the study area offshore Rotterdam, immediately south of the approach channel to the Port of Rotterdam, and shows depths of the pits compared to the surrounding bed elevation.

The surrounding seabed is characterised by tidal bedforms (Figure 2): shoreface-connected ridges from the pits south-westward, parallel to the shore, and flow-transverse sand waves superimposed on the banks and farther offshore.

2 Methods

In order to map the sea-bed sediments of the MV2 sand pit with acoustic bed classification, a hydrographic survey was conducted, acquiring both bathymetric and backscatter data. For the sediment mapping, acoustic classes need to be coupled to sediment characteristics, as determined from sea-bed samples (ground truthing). We opted for box coring, because the backscatter strength is thought to be determined by the sediment characteristics at the bed surface, such as grain size and sorting, but also by the presence of thin veneers of contrasting sediment, shells and protruding macrobenthos, and possibly by the very shallow subsurface materials or layering (down to a few centimeters). A box corer allows for taking undisturbed bed samples, thereby preserving the surface characteristics and subsurface layers, as well as *in-situ* shells or macrobenthos at the bed, unlike for instance Van Veen grab samples, in which bed samples are mixed and the surface and subsurface layers are not preserved. The penetration depth of a box corer in sandy and muddy sediments is a few to several decimeters, which is sufficient for investigating the shallow subsurface.

2.1 Offshore hydrographic survey

2.1.1 Multibeam bathymetry and backscatter data

Hydrographic data of the MV2 sand pit were acquired aboard the RV Arca of Rijkswaterstaat on the 12th - 14th of November 2018 (week 46), using a hull-mounted, dual-head Kongsberg EM 2040C Multibeam Echo Sounder (MBES). The data were acquired in both QPS Quinsy software and Kongsberg SIS software. Qinsy is the software standardly used aboard the RWS vessels for hydrographic data acquisition and these data can be used in an easy workflow for bathymetry, and SIS-data store all data that are required for the analysis of the multibeam backscatter data per beam in the Bayesian bed classification method used in this study.

The main multibeam acquisition settings were:

- a constant pulse type (continuous wave, CW) with a pulse length of 145 μs,
- a constant center frequency of 300 kHz (due to dual head configuration frequencies switch between 290 and 310 kHz),
- a constant swath coverage of -5 to 65 degrees for starboard and port sides,
- an angular coverage mode: manual
- a single swath mode
- a maximum and constant TX power level
- an equiangular mode (i.e. constant beam spacing)
- a normal incident sector of 25 degrees (constant)

In SIS software, all settings need to be entered manually. For the full list of multibeam settings, see the survey plan (Products\survey plan.pdf). Data in this study are presented in UTM31N ETRS89 co-ordinates.

At the start of the hydrographic survey, a calibration line was sailed for the height of the MBES, which showed a difference of 3 to 4 cm with the previous survey. The distance of the RTK and hull-mounted MBES aboard the MV Arca is standardly set for acquisition software in Quinsy; the settings for SIS were manually imported. A sound velocity profile (SVP) was measured with a probe (Table 1 in section 2.1.2). The mini-SVP in the MBES system (SVS) measures sound speed every 1 second; in case of a system warning, the SVP will be measured with a probe.

In collecting the MBES data, surveying started at the northern excavation pit, proceeding southward. In the northern pit, the spacing between tracks was kept as planned, since with less overlap, voids in the data appeared for the shallow areas around the pit. Tracks were sailed in east-west course, partly to reduce sailing time but also because of the vicinity of the approach channel to the Port of Rotterdam. Tracks were sailed as straight as possible, at a speed of 6 knots for high resolution, with an overlap of 110% to avoid gaps and a line spacing of 38 m. (N.B. 1 line was sailed at 9 knots and is noted in the survey report and logged in the data files.) The MBEs ping rate was as high as possible with given water depths and swath width for high-resolution data.
During the survey, a horizontal positioning error was observed in the data, due to an erroneous setting in the distance between the GPS and the MBES head in the SIS software only (not in Qinsy), about 2/3rd in in the survey of the northern pit. We corrected the settings on board (-13 m instead of +13 m) from line 29 in the survey report onwards. We tested the corrected settings by visually inspecting two adjacent back-and-forth sailed lines, and no offset was observed. In QPS software, the data can be replayed to correct for settings, but SIS data, which stores the beam-forming data that is required in the bed classification method, cannot be replayed. Tracks are logged in the data files and the erroneous data were corrected for horizontal positioning in the pre-processing (section 2.4.1).
For the southern pit, survey lines were recalculated on board, with slightly larger spacing between the tracks and were sailed with increased speed, in order to optimise the survey time whilst guaranteeing data quality.
The order of the sailing tracks was variable throughout the survey: sometimes sailing back and forth of adjacent lines (opposite directions), and sometimes in larger loops, to reduce turn times (logged in the data).

Three cross lines were sailed (two in the N-pit and one in the S-pit) for evaluation of the MBES-data.

For the MBES bathymetry data, sound velocity profiles are sufficient, whereas for the backscatter data, conductivity, temperature and depth (CTD) measurements are necessary for calculating sound absorption (section 2.1.2).

All hydrographic data were copied onto external hard discs provided by Deltares.

2.1.2 Water-column data

Four conductivity, temperature and depth (CTD) measurements were done with a Seabird SBE model 11-plus CTD deck unit for the calculation of sound speed, signal refraction and absorption in the water column. Table 1 provides an overview of the SVP and CTD measurements conducted.

SVP	*CTD*
12-Nov-2018 13:45	12-Nov-2018 15:45
12-Nov-2018 16:07	
	13-Nov-2018 11:30
	14-Nov-2019 16:00 (off in salinity)
	14-Nov-2019 18:00 @ South-pit

Table 1: Overview of sound velocity profiles (SVP) taken with probe and conductivity, temperature and depth (CTD) measurements.

Water samples of 2 liters were taken near the seabed four times during the survey with the sampling tubes on the CTD probe. Samples were completely clean, without any sediment. After settling in the lab, no residue – neither sediment nor organic – was observed at the bottom of the samples (suspended sediment concentration of 0 g/l). Therefore, sediment concentration analyses of these samples were not conducted and locations and timing with respect to the tide are not noted in this report.

We also collected 1 track with multibeam backscatter data of the water column (in Qinsy software only; no licence available for SIS), separately from the survey, and merely as a pilot for future use. These data are not described in this report.

2.2 Sea-bed sampling: box cores

The selection of sampling locations was aimed at both mapping seabed sediments in the pits and testing the discriminative performance of the MBES backscatter measurements in these areas. In order to be able to assign sediment characteristics to the backscatter strengths in the best way possible, locations of box cores were determined on board, based on the first inspection of the preliminary backscatter results acquired in the survey days before, in order to represent the variation in backscatter strengths in the excavation pits and the surrounding seabed. Box cores were thus taken during the same campaign, in order to minimise any changes to the seabed over time. 21 Box cores were taken, which could be done in 1 day of survey time (15th of November 2019), and are believed to represent the zones of varying backscatter adequately, with 2 samples (bare minimum) in two of the high-backscatter zones and up to 4 in the northern pit and 5 in the surrounding seabed. In smaller areas of contrasting backscatter, one box core was taken. For location of the box cores, see Figure 12.

Two cylindrical box corers of RWS were used, both with a diameter of 31.5 cm (Figure 3a). Sub-cores were taken for description of subsurface sediments by inserting PVC liners when the cylinder was still in place. Photos were taken from the surface when the cylinder was removed for additional descriptive characterisation of the surface and macrobenthos (Figure 3b). Since the photos could not be taken before inserting the PVC liners, due to reflection in the remaining water in the cylinder that obscured the sedimentary surface, we did not take vertical photographs in this case (which would have allowed for quantification of shell-covered surface by image analysis in a more detailed study).

(a) *(b)*

Figure 3: (a) Cylindrical box corer of RWS aboard the MV Arca. (b) Box core as taken from the seabed, with PVC tube for sub-core for the description of subsurface sediments in the laboratory. (Note the contemporary sample number label)

Because coarse-grained material, such as shells or gravel, at the surface or just below the surface may affect the backscatter strengths, and since it is statistically more correct to

determine gravel content from larger samples (small samples may miss larger grains or shells, or merely contain one larger grain or shell), we sampled the top 7 to 10 cm of the remaining surficial sediments around the PVC tube in the box cores on board, so that we had samples of 1 to 1.5 kg.

Sub-cores and samples were shipped to Deltares in Utrecht to be described and analysed, respectively, in the laboratory.

2.3 Description of sub-cores and grain-size analyses (laboratory)

The box cores were opened, photographed immediately after opening and geologically described by Deltares in the laboratory of TNO Geological Survey of the Netherlands. Lithological descriptions of the sediment cores and grains-size analyses were conducted according to NEN-5104 standards, which aim to describe sedimentary characteristics that are relevant in geological and applied geological studies in a univocal way. In addition, special attention was paid to surface characteristics that may affect the backscatter strength, such as mud veneers, shells and protruding macrobenthos.

2.3.1 Lithological description of the sediment cores (NEN-5104)

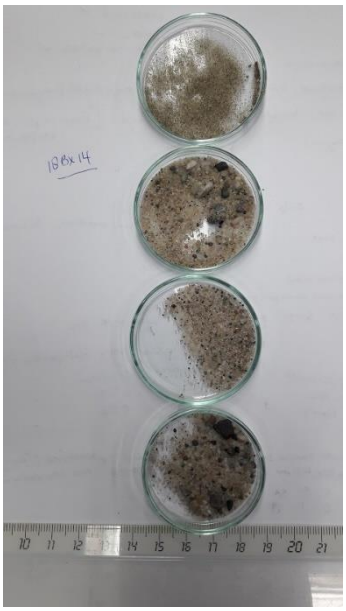

In the lithological descriptions, the organic, carbonate and siliclastic sediments are divided in four fractions by grain size: clay, silt, sand and gravel, following the Wentworth classification (Table 2). Most samples are a mixture of different fractions, which together determine the lithology. The analysed cores comprise gravel, sand, silt and clay, organic matter, and shells or shell fragments. In the description, different layers in the sediment cores are distinguished, for example a main layer (e.g. *'sand'*), sublayers (e.g. *'with clay laminae'*), type of mixture (e.g. *'very silty'*), and additionally included material (e.g. *'trace of organic material'*). Median grain sizes were estimated using a comparison microscope, by which the sediment (Figure 4) is compared to digital example photographs of grain-size classes. Calcium content was determined with HCl on the described half of the core.

Figure 4: Four samples of BX14 for estimating median grain size under the comparative microscope.

grain size	***name of fraction***
< 2 µm	Clay
2 µm - < 63 µm	Silt
63 µm - < 2 mm	Sand
2 mm - < 64 mm	Gravel

Table 2: Fractions and grain-size classes, following the Wentworth classification (Wentworth, 1922), as used in the lithological description of box cores and grain-size analyses.

Mud content

The presence of mud (grains < 63 µm; i.e. clay and silt) is visually determined by rubbing the sediment between one's fingers and observing the fine fraction that coheres to the hand. Estimates of mud content were determined using a comparative microscope. The sediment is then classified according to the mud content (Table 3). For a more accurate and quantitative

determination of the mud content, laboratory measurements of grain-size distributions were performed on sub-sampled layers.

Table 3: Mud content classes

percentage mud	***terminology***
< 10	slightly silty
10 - < 17,5	moderately silty
17,5 - < 32,5	strongly silty
32,5 - < 50	extremely silty

Gravel content

The gravel content (% grains > 2 mm) classification is as listed in Table 4. For percentages smaller than 50%, gravel is the fraction mixed in the main fraction, e.g, gravelly sand. For percentages above 50%, gravel becomes the main lithological fraction, e.g. sandy gravel. The subdivision in the gravel classification applicable to the sediments in this study is only as mixed in fraction and therefore terminology over 50% is not included in Table 4.

Table 4: Gravel content classes

percentage gravel	***terminology***
< 10	slightly gravelly
10 - < 20	moderately gravelly
20 - < 50	strongly gravelly

Shell content

In the descriptions of the shell content, the total amount of shell material is taken into account (Table 5). The shell content is not standardly described in detail, since for that, all shells need to be sieved from the core and be classified. In this study, however, we did make note of shells at the surface.

Table 5: Shell content classes

percentage shell material	***Description***
0	No
> 0 - < 1	Trace
1 - < 10	Few
10 - < 30	Many

Stratigraphy

No stratigraphy was attributed. However, mention of a few stratigraphic layers is made in the interpretation of the sedimentology, merely to identify similar deposits in the cores in this study (Bligh Bank Formation [Holocene marine deposits] and Kreftenheije Formation [Pleistocene gravelly meltwater deposit]), which latter was verified with a Quaternary Geologist at TNO.

Additional descriptions (non NEN standard)

Since surface characteristics may affect the backscatter measurements, we additionally described surface characteristics, such as the presence of a thin mud veneer layer, shells or live macrobenthos at the surface, protruding macrobenthos, etc.

2.3.2 Grain-size analyses

For detailed analyses of grain-size distributions, each sediment core was subsampled in one half of the core at the surface (0 – 1 cm for most samples, except for where insufficient sediment could be sampled, 0 – 2 cm was used) and analysed in the joint laboratory ‘Castel’ of Utrecht

University, Deltares and TNO Geological Survey in Utrecht. Thin mud veneers at the surface of some cores were too thin to sample separately (a minimum of 25 g of sediment is required), so that the mud is included in the resulting grain-size distributions. In sediment cores with different lithological layers, subsamples were also taken at depth to characterise those layers. The depths intervals of all samples are specified in the Excel sheet with full grain-size analyse data provided with this report (Products\Malvern results.xls).

The larger samples, that were taken for gravel content, were sieved at the laboratory of Deltares in Delft.

2.3.3 Grain-size distributions of sediment cores

Form each sub-sample, the grain-size distribution was determined by laser diffraction, a technique that measures the scattering of light. Because sediment grains of different grain size scatter the laser beam into different angles, the variation of angles and light intensity is a measure for the grain-size distribution of the sediment.

All samples were dried in an oven at 80 °C. For the grain-size analyses, the following steps were conducted:

- careful disintegration of aggregates in a mortar (whole shells are maintained),
- removal of particles larger than 2 mm with a sieve,
- sub-sampling (0,5 – 5 g) with a splitter,
- preparation of the subsample with a hydrogen peroxide (H2O2) solution for the removal of humus,
- preparation of the subsample with a hydrochloric acid (HCl) solution for the removal of carbonate and other salts,
- to peptise the sample with pyrophosphate to prevent aggregation,
- to disperse the sample to a concentration that is suitable for further analysis,
- to analyse the sample (< 2 mm fractions) with a Malvern Mastersizer 2000,
- to calculate the volume percentages from the raw signal with a model based on predictive theories for light scattering and absorption by particles. Each raw signal is a compilation of many subsequent measurements of the scattering of light in the sample.
- And to calculate median grain sizes, sorting and cumulative distributions of the sediments.

The measurements were conducted without application of ultrasone conditions (extra disintegration of aggregates within the Malvern-apparatus).

2.3.4 Sieving of larger samples

Grain-size distributions of the larger samples were determined by sieving. Samples were dried in an oven at 50 degrees, fined in a mortar, resampled to samples of around 300 g, weighed and sieved over a stack of 18 sieves with reducing mesh sizes from 2 mm according to NEN-5104 standard (Figure 5) for 20 minutes on a shaking device with 10-seconds intervals.

2000
1400
1000
710
500
355
250
212
180
150
125
106
90
75
63
53
38
1

Figure 5: Photo of the sieves and shaking table (on the right), with mesh sizes of stack of sieves used for the larger samples < 2000 μm (in μm) on the left (according to NEN-5104 standards).

Residues on the sieves were weighed and the through-fall calculated in cumulative weight percentages. The maximum difference of the sum of weights and the total weight at the start of the analysis is 0,4 g for an adequate measurement.

To determine the distribution of larger fractions, the samples BX12 and 16 were sieved over a stack of sieves with larger mesh sizes: 16, 10, 8, 4, 2 and 0.1 mm. The other samples did not contain much gravel of these grain sizes (since these larger samples do not include the deeper sand-and-gravel layers in BX 8 and 14 that were interpreted as Krefteneije Formation, see section 3.3).

2.3.5 Sediment type Folk classifications

In the literature describing the Bayesian bed classification method [e.g. Simons & Snellen, 2009; Gaida et al., 2018a; 2018b; Snellen et al., 2019], most comparisons of acoustic bed classes to sediment type use Folk classes. In order to be able to compare performances of this study to the literature, we added Folk classes in our study as well. Based on the grain-size distributions in the laboratory (Malvern analyses), we classified sediment type, using Folk's [1954] diagrams (Figure 6). We recalculated the percentages of the cumulative Malvern analyses (< 2 mm) to include the > 2 mm fraction. Since each of the samples in this study contained more than 0.01% (trace) of gravel, classifications were done based on the gravel-sand-mud fractions diagram on the left in Figure 6.

If we would have classified the samples of the < 2 mm only (Malvern analyses), using the triangular diagram on the right in Figure 6, then all samples would classify as Sand (S), since all samples contain more than 90% of sand, irrespective of the silt and clay contents. Besides, when testing the sea-bed sediment mapping using acoustic bed classification, analysing all fractions makes more sense scientifically, since the backscatter measurements at the seabed measure the full content of the sea-bed sediment composition.

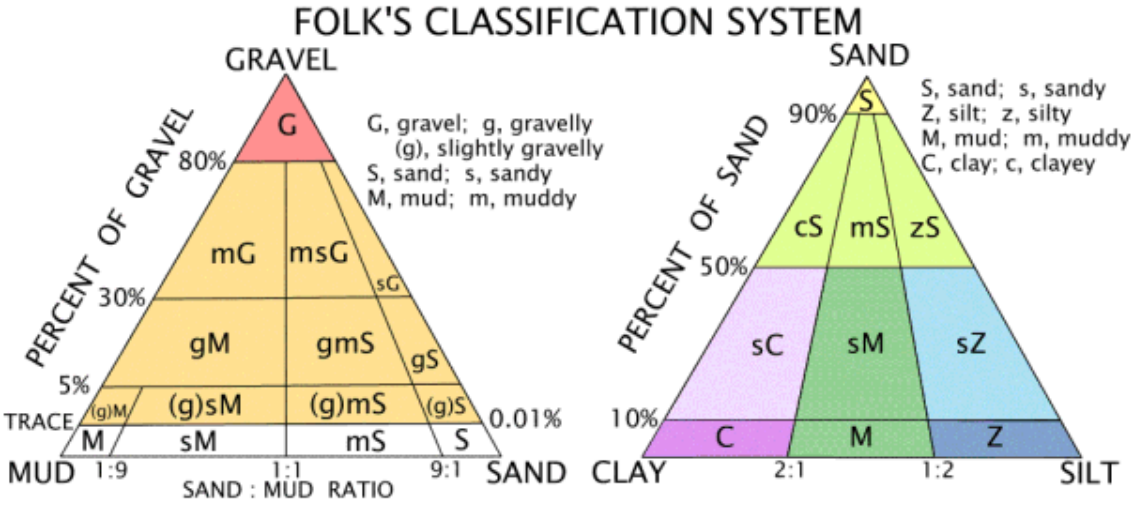

Figure 6: Folk [1954] sediment classification diagrams for sediments containing gravel (left) and for the sand-silt-clay fractions (< 2 mm).

2.4 Acoustic sediment classification

In this section, we describe the pre- and post-processing of the MBES data, the acoustic bed classification with the Bayesian technique developed by Delft University of Technology and the sediment mapping of the study area.

2.4.1 (Pre-)processing of the multibeam backscatter data

In the pre-processing, we corrected for the horizontal positioning error in part of the MBES data stored in the SIS software, due to erroneous settings on board of the distance between the GPS and the MBES head, using the log data. The backscatter data were corrected for transmission loss, i.e. absorption and spreading, and the seabed morphology based on the sonar equation (Equation (1) in section 1.2). In correcting for seabed morphology, the actual slope angles of the seabed are calculated from the MBES bathymetry data, which are then used to correct the incident angles of the beams to true incident angles. Having obtained the corrected BS signals, we can use these to classify the seabed (post-processing).

2.4.2 Acoustic bed classification

Measured backscatter strengths are affected by random fluctuations of the acoustic interaction with the seabed [Lyons & Abraham, 1999] and thus can be considered as a random variable with a certain mean and standard variation. According to the central limit theorem, measured backscatter strengths per beam, which are determined as the average over backscatter from the scatter pixels within a beam (backscatter time series), can be assumed to follow a Gaussian distribution [Simons & Snellen, 2009] as long as the averaging is done over sufficient statistically independent scatter pixels. A scatter pixel represents the instantaneously ensonified area of the seafloor by the transmitted pulse of the MBES, i.e., the signal footprint. If the frequency and angle of incidence are constant, the backscatter strength is dependent on the seabed properties. Thus, if the survey area contains m different sediment types, the backscatter histogram for a selected beam can be represented by a combination of m Gaussian distributions (Figure 7).

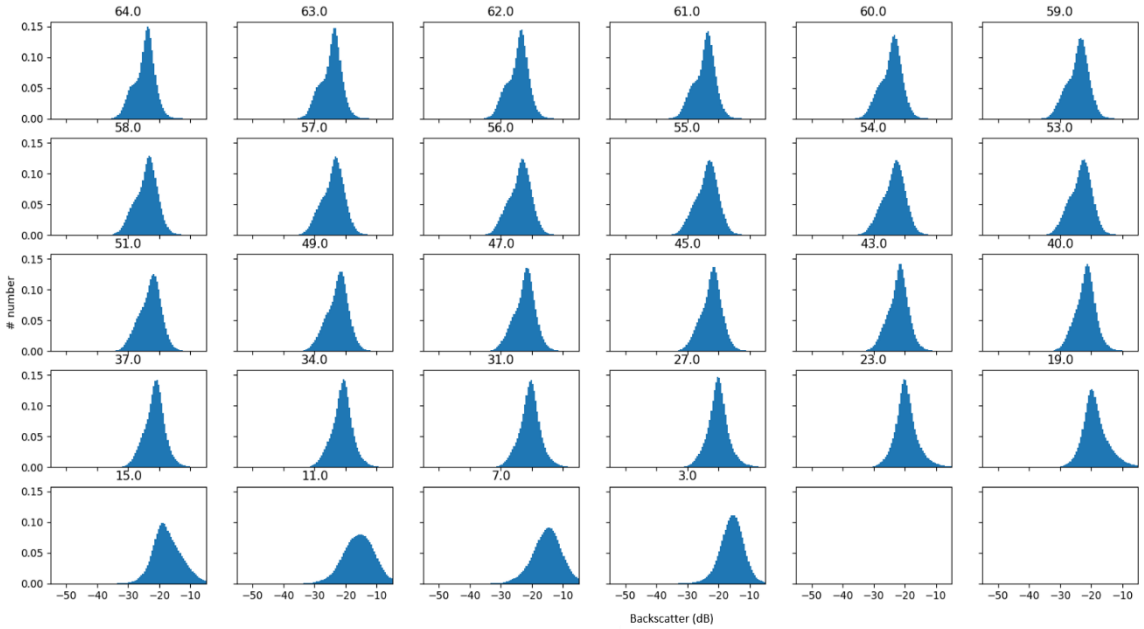

Figure 7: Histograms of backscatter values (dB) per beam for selected beams of 64° down to 3°.

The actual classification is based on the Bayes decision rule. In this case, m states or hypotheses, indicated as H_k with k = 1, . . . , m, exist. These hypotheses correspond to the m seafloor types present in the surveyed area. In the following, the Bayesian decision rule for multiple hypotheses is used to define which hypothesis is accepted, i.e.,

$$\text{accept } H_k \text{ if } \max\{ f(y_j|H_i)P(H_i)\} = f(y_j|H_k)P(H_k) \quad (9)$$

where $P(H_i)$ is the *a priori* probability of hypothesis H_i with i = 1, . . . , m. Considering that the measurements are taken for the first time, all hypotheses are equally likely, which results in $P(H_i) = 1/m$. The decision rule is then simplified to

$$\text{accept } H_k \text{ if } \max\{ f(y_j|H_i)\} = f(y_j|H_k). \quad (10)$$

Therefore, the hypothesis that maximizes the likelihood $f(y_j|H)$ is selected for observation y_j. The intersections of the m Gaussians have thus to be determined, which results in m non-overlapping acceptance regions, A_k defining the so-called acoustic classes (ACs). The boundaries of the ACs are determined for a certain number of reference angles (mostly outer beams). The reference angles are selected based on three requirements: (1) providing most consistent results in terms of the location of the Gaussian distributions per dataset, (2) offering high discrimination power (30° to 70°), and (3) containing less noisy data. Based on the percentage distribution of the ACs at the reference angles, the ACs are assigned to the backscatter data at all considered angles (mostly 10° to 60°). In this study, the method returns for different examined beam angles the fitting of 3 to 8 Gaussian distributions and the corresponding Chi-square value, X^2. Based on this X^2 value, the method finds the optimal number of acoustic classes to represent the measured backscatter data. Here we plotted the 40°, 54° and 64° beam angles as an example in Figure 8. For more figures, see Appendix 1, of which the resulting number of classes are summarised in Table 6.

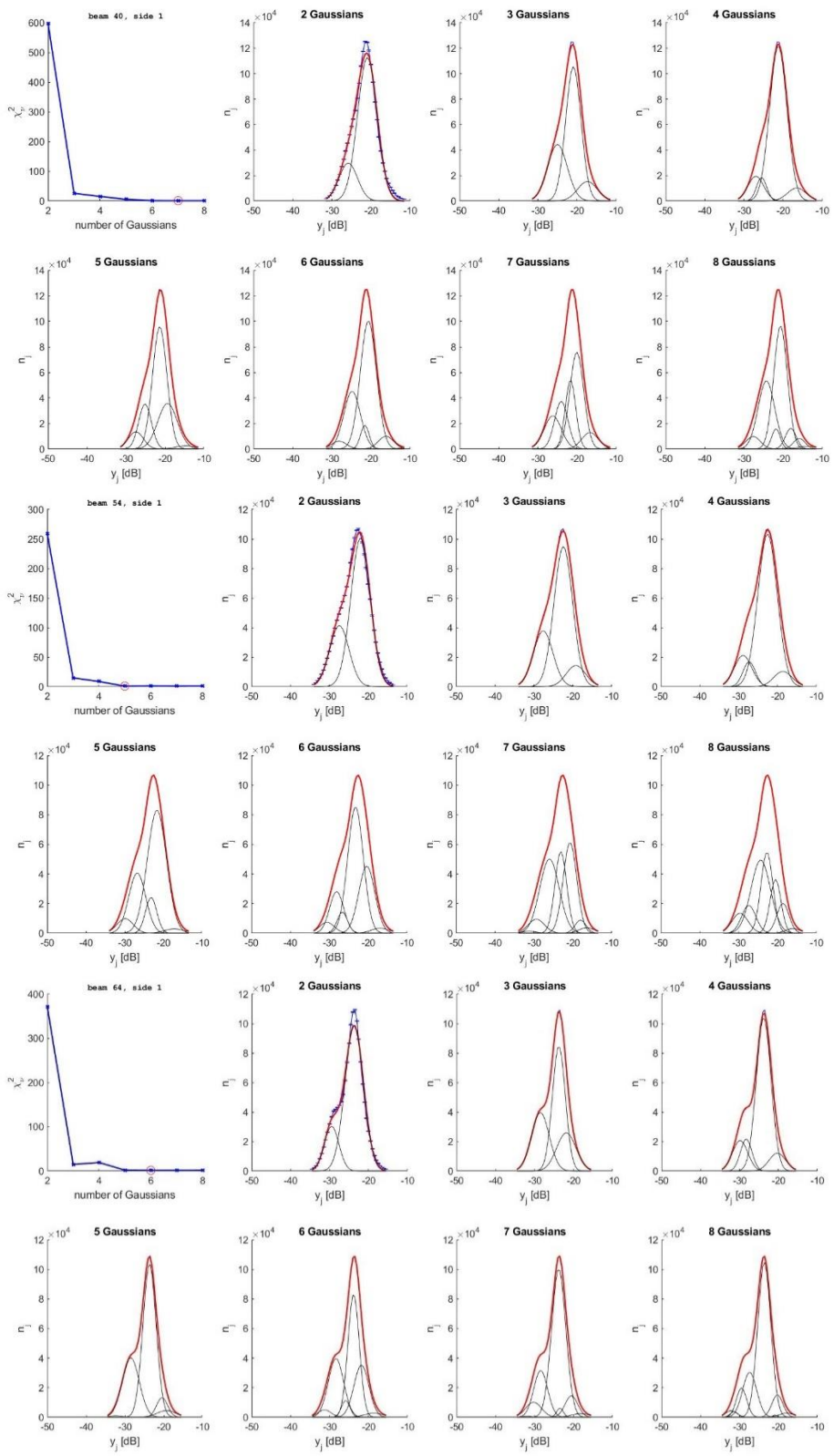

Figure 8: Plots of bed classification calculations for MBES beams 40°, 54° and 64°, and approximations of the measured (corrected) backscatter curves with 2 to 8 acoustic classes (Gaussians). In each figure, the first plot displays the number of classes as recommended by the method (red circle on blue line), which are summarised for all examined beam angles in Table 6*.*

Beam angle	No. of classes	Beam angle	No of classes
37	7	60	5
40	7	61	5
45	7	62	7
51	5	63	7
53	6	64	6
54	5		
56	5		
58	8		

Table 6: Number of acoustic classes calculated by the method to be the best approximation of the corrected MBES signal. See Figure 8 for examples of 40°, 54° and 64° beam angles or Appendix A for all plots.

These tests of bed classifications, using different ranges of MBES beams and different number of classes in the method, revealed that, from all angles, the outer beams are the most discriminative for conducting the bed classifications. Thus, we used as reference angle the average angle of 54, 56 and 58 degrees to estimate the number of classes. The optimal number of classes, as determined by the method, is based on the value of the reduced X^2, where a value close to 1 indicates a good fit (Gaida et al., 2018b). Visually, the kink in the curve (Figure 8 and Appendix 1) indicates that the improvement of the classification with increasing classes to the right of the kink, is small. The outcomes of the X^2 tests provide the optimal number of classes, which in this study is between 3 and 8 classes (only beams in Appendix 1 are mentioned in Table 6). Although the decisions in this study follow the methods and settings by Gaida et al. (2018b), in which a detailed flow chart can be found, this range in classes is larger than the normal outcomes in earlier studies. The influence on the outcomes of the more subtle changes in the sediment characteristics than in the earlier studies described in the literature, remains to be investigated.

The analyses of the MBES data were done on the beam angle range of 20 to 64 degrees of both starboard and port sides and the bed classifications that we performed were for 3, 4 and 5 classes. The generated maps with 3, 4 and 5 classes, are shown in Figure 9, Figure 10 and Figure 11, respectively, for illustration reasons only. Choices on the number of classes follow in the results chapter.

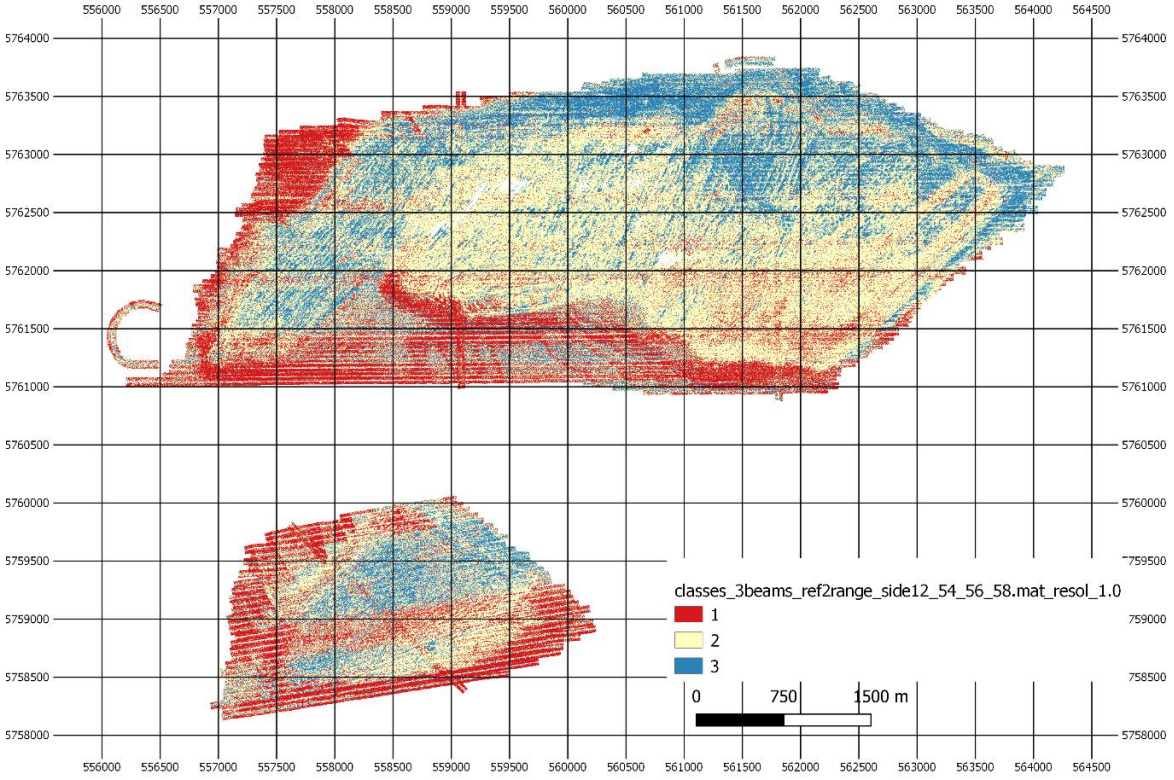

Figure 9: Acoustic bed classification with 3 classes.

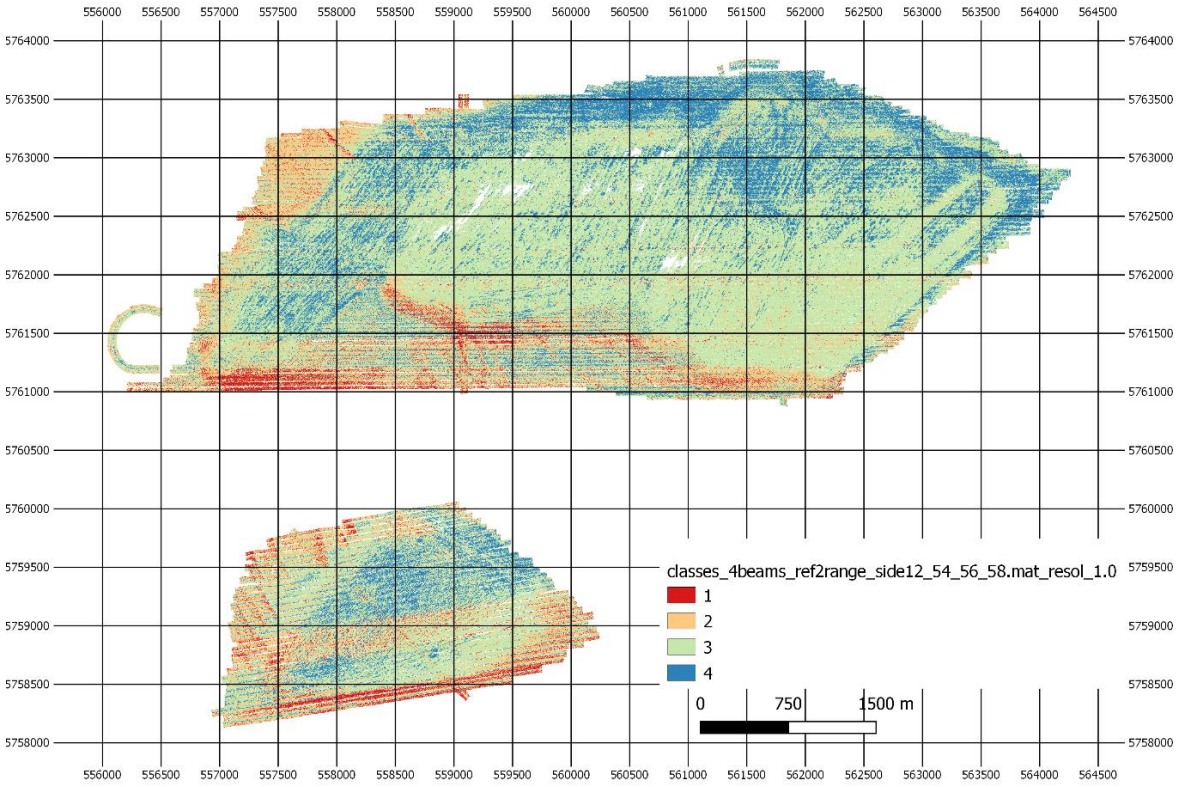

Figure 10: Acoustic bed classification with 4 classes.

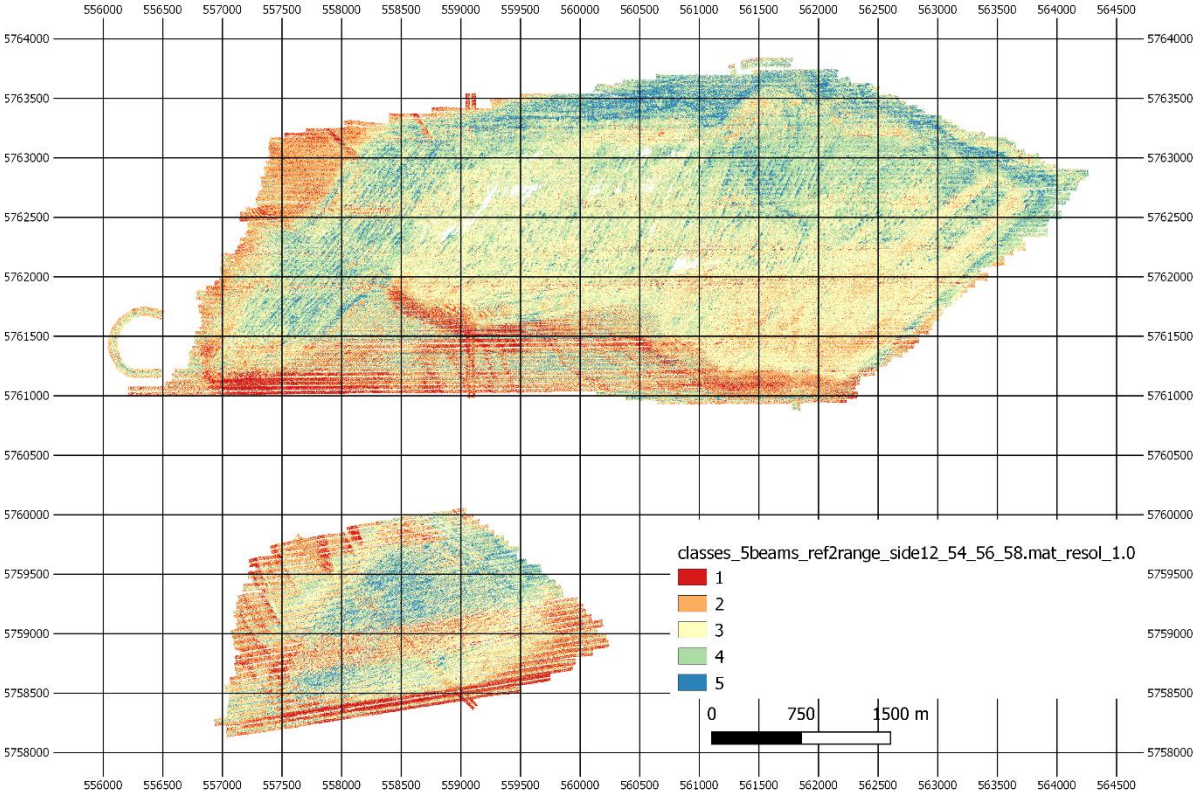

Figure 11: Acoustic bed classification with 5 classes.

2.4.3 Sediment mapping

Sediment mapping is achieved by assigning sediment type to the obtained bed classification map in the previous section, using box cores. Since box core locations at the bed are not necessarily precisely the x,y coordinates of the sample locations (due to displacement of the box corer by the tidal current), we resampled the acoustic bed class (ASC) from the bed classification maps as average in an area around the coordinates. Hereto, we tested the effect of variability in classes/pixels, by comparing the resampled average class for different search radii (0.5, 1, 2, 5, 10 and 20 m). In the results chapter, we use the average class within a 2-m radius, since this seems a realistic distance of precision of the box corer.

In this study, we did a detailed study of grain-size characteristics of the box core samples. We correlated the acoustic classes not only to Folk classes of sediment type, but used different quantitative parameters from lab analyses, such as median grain size (d50), mud content, sorting (both measures d60/d10 and d90/d10), as well as descriptive parameters of sediments at the surface, such as the presence of coarse material (shells), thin veneers of mud, or a high density of macrobenthic species, either or not protruding from the bed. We used on-board descriptions and sediment cores, and photographs and lab results, to describe the latter parameters.

Correlation plots of the resampled, average ASCs to the sediment characteristics provides an evaluation of the assignment of sediment characteristics to ASCs.

3 Results and interpretation

3.1 Seabed morphology and backscatter mosaics

Water depths in and around the sand extraction pits for Maasvlakte 2 range between 18.7 m and 47.5 m below LAT (Figure 12). The surrounding seabed is at a depth of 18 – 27 m and is characterised by tidal bedforms (megaripples and sand waves). The depth of the northern (main) extraction pit ranges from more than 30 m to 47.5 m. The southern extraction pit is much smaller and less deep, with water depths up to 38 m. In both pits, the bed morphology displays dredging marks.

Backscatter results (corrected for water column effects and bathymetry) reveal clear zones of varying backscatter strength (grey scale in Figure 13), where darker grey tones represent lower backscatter and light grey tones represent higher backscatter. The range of all values in decibels (dB) is from approximately -42 dB to -10 dB for the entire study site and the MBES backscatter measurements are able to pick up the differences in sediment characteristics. The surrounding seabed exhibits the darkest two grey tones of low backscatter, whereas the bottom of the pits reveals the intermediate and lighter grey tones of higher backscatter, with the highest backscatter values in the western part, the northern edge and areas in the north east of the North-pit, and in the South-pit. In the southern pit, a bundle of sailing tracks shows up as darker toned; this is a data artefact, which could be caused by different conditions (weather, sea state) or by the RTK, GPS and MBES systems. Bundles like these were observed in earlier datasets (e.g. Kustgenese 2 data Ameland, surveyed with MV Arca) as well; for determining the exact cause of this artefact, the data need to be studied in more detail.

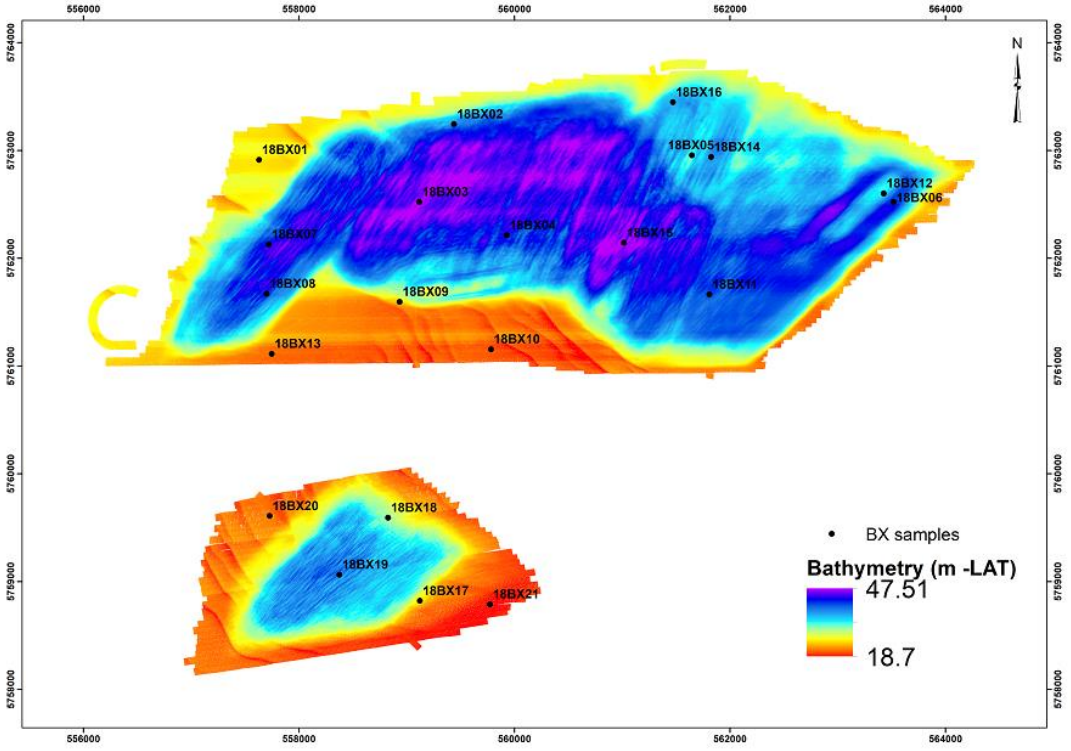

Figure 12: Bathymetry map of the sand extraction pits Maasvlakte 2, offshore Netherlands. Locations of the box core samples are indicated. Co-ordinates are in UTM31N ETRS89.

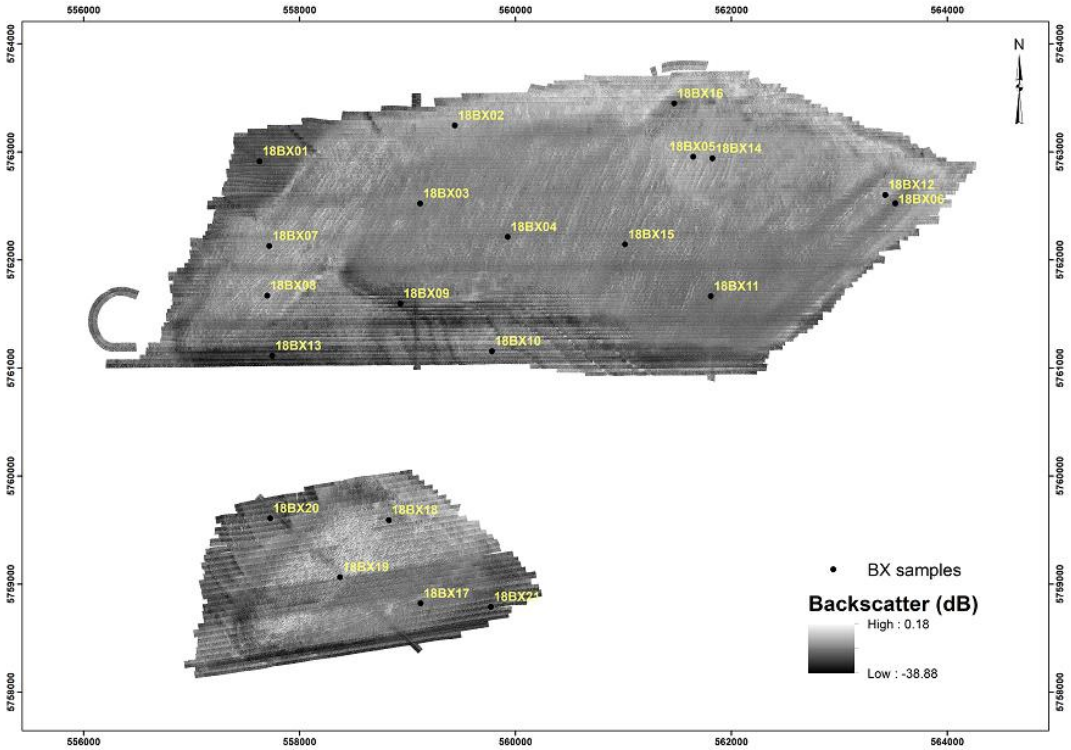

Figure 13: Backscatter mosaic of measured MBES backscatter values, exhibiting the lowest BS-values on the surrounding natural seabed (dark in map) and intermediate and highest backscatter values in the excavation pits. Box core locations are indicated. Co-ordinates are in UTM31N ETRS89.

3.2 High-resolution acoustic bed classification

Based on the tests of bed classification results, using different ranges of MBES beams and different numbers of classes in the method (section 2.4.2), we opted for the bed classification results with 4 classes (Figure 14). For some beam angles, the optimal number of classes was 4 and herein, we're following the general principle to choose the least number of classes (simplest solution) to not overinterpret. In the correlation plots (presented in section 3.5) it is displayed that the only difference between 3 and 4 classes is that samples BX9 and 13 are allocated to a separate class, which indeed increases the correlation. For making these choices in a more robust way, more thorough testing and interpreting needs to be done, which is beyond the scope of this project.

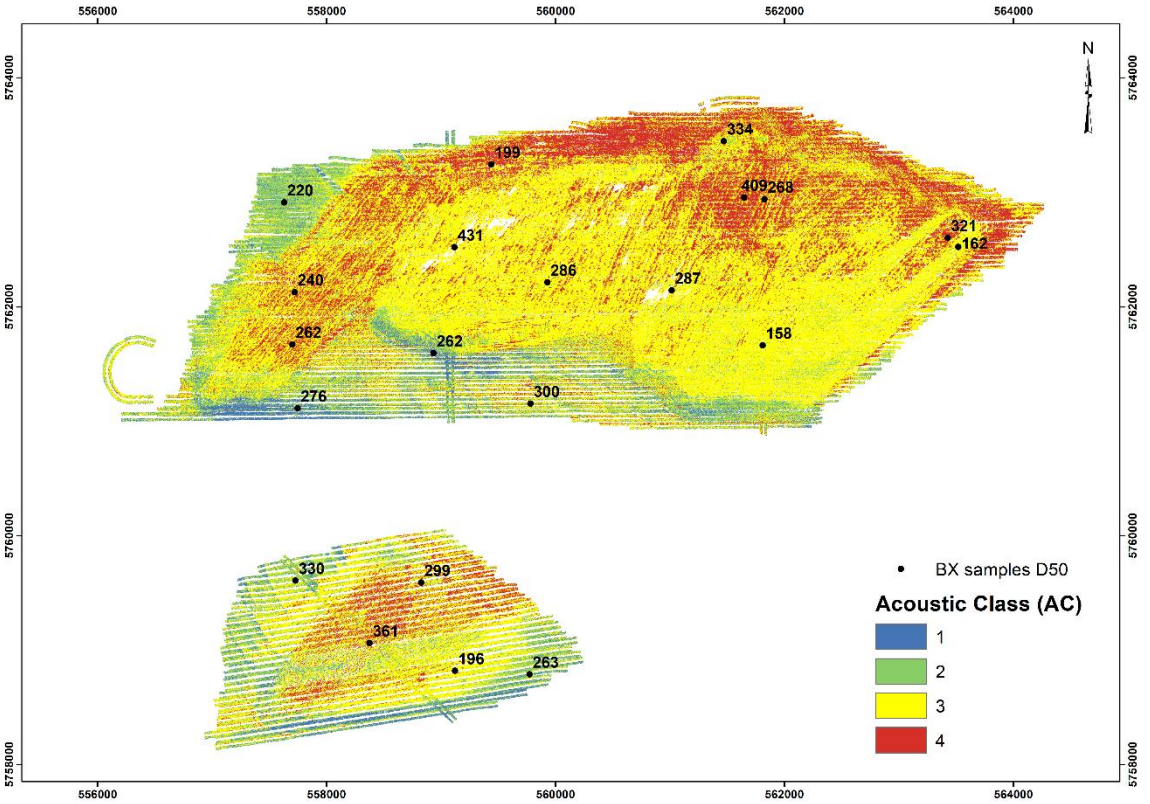

Figure 14: Resulting high-resolution map of acoustic bed classification, showing 4 acoustic classes (ACs), based on measured (corrected) backscatter strengths. The locations of the box cores are indicated and labelled with median grain size (d50). Co-ordinates are in UTM31N ETRS89.

Assignment of sediment characteristics (presented in sections 3.3 and 3.4) to the acoustic classes in this section results in a high-resolution sediment map, which is presented in section 3.5.

3.3 Sediment core descriptions (box cores)

The box cores are displayed in the photographs below (Figure 15). The box cores of the surrounding seabed (BX 1, 10, 13, 20 and 21) exhibit nearly massive beds of clean (0% mud), brownish, marine sand, interpreted as the Bligh Bank Formation (Holocene marine sands). BX13 and BX21 are the nicest example of a massive sand layer. In some cores few dark-coloured mottles of bioturbation by macrobenthos occur. Exception on the clean sand is BX1, which contains a small amount of mud (see Table 7). BX10 has a thin mud drape at the surface, a higher shell content and a darker layer at 11 cm depth, which may be due to bioturbation and

oxygen depletion, but also contains more red and black sand grains, so could be interpreted as a separate layer of different composition.

Figure 15: Photographs of all 21 box cores.

Many of the cores from locations in the sand extraction pits have similar marine sands at the surface, but are more (slightly) silty. Below this top layer, cores with slightly silty sand in the pits show darker (oxygen-reduced) units that are more strongly bioturbated (e.g. BX2 – 4 and 7). BX8 (western part of N-pit) and BX14 (north-east part of N-pit) display coarser gravelly sand layers at 6 to 8 cm below the surface, with clasts up to 30 mm, which are interpreted as the top of the Kreftenheije Formation (Pleistocene glaciofluvial deposits) (pers. comm. Freek Busschers (TNO Geological Survey of the Netherlands)). Cores 6 (in dredged track in the east of the North pit) and 11 (east-part of N-pit farther south) comprise fine-grained sediments. BX6 penetrated 60 cm (i.e. the full length of the cylinder). BX6 was selected in a dredged track (deeper) and in a zone of low backscatter, and below a 0.5 cm thin top layer of silty sand, it contains a 40 cm thick clay layer. The sandy layer below the clay layer may be the original bed. At 20 cm in BX6, a piece of bone (?) was found (Figure 16). BX11 contains a clay layer at 6.5 – 12 cm depth, overlain by a slightly silty sand layer.
The lithological descriptions of the sediment cores are documented and will be imported in the application BORUS and will be made available in the public DINO database (Data and Information on the Dutch Subsurface) of TNO Geological Survey of the Netherlands and are provided in the digital products with this report (Products\box core descriptions.pdf).

Although not visible in Figure 15, after drying out of the core surface during description, BX8 (in Kreftenheije deposits below sandy top layer) and BX19 (S-pit; Figure 17) showed cross lamination (in BX19 in two different layers with a boundary at 15 cm depth).

Of the box cores in the sand pits, BX9 (upper slope of the N-pit) and BX16 (northern patch of N-pit) are very similar to the sediments of the surrounding seabed.

Figure 16: BX6, with on the 20 cm boundary between clay beds, a piece of bone? (unidentified), of about 3 cm wide.

Figure 17: BX 19 (S-pit), showing cross lamination in two different layers.

Surface characteristics of the box cores were variable. Mud drapes occur on BX2, 5, 7, 9 (partial drape on BX9), 10, 15, 17 and 18 (partial drapes on BX17 and 18), of which BX2 and 7 are very thin (<<0.5 mm), and BX10 and 15 are continuous mud veneers (Figure 18). The thickest mud veneer on BX15 (Figure 18d) is approximately 1 mm thick. Some surfaces were slightly rougher due to coarser grains, shells and/or tube worms (e.g. BX5, 12 and 14). BX 4 and 11 have a more bumpy surface (higher roughness); the bumps in the fine-grained BX11 is caused by a large number of young/small sea urchins in the top 2 cm. Flat and bare sand surfaces were observed in several box cores, with the even surface in BX13 (Figure 18b), 20 and 21 (all three in the surrounding sea bed).

(a)

(b)

(c)

(d)

Figure 18: Examples of different surface characteristics of the box cores. (a) mud veneer of BX10 in the surrounding seabed; (b) clean-sand surface of BX13 in the surrounding seabed; (c) rougher seabed of BX12 (on rim between dredging trenches in N-pit); (d) mud drape and 1 protruding tube worm at BX15.

3.4 Grain-size characteristics

Grain-size distributions of the subsamples from sediment cores, as described in the previous section, are expressed in cumulative volume percentages based on the Malvern analyses of samples with the < 2-mm fractions. The grain-size distributions of the larger samples, determined by sieving, result in cumulative weight percentages of all fractions. These results cannot be combined or directly compared. Therefore, grain-size results are described in two separate sections.

3.4.1 Mud and sand fractions (Malvern analyses)

For the surficial sediment samples, median grain sizes of the mud and sand fractions (< 2 mm; Malvern analyses), range from 158 – 431 μm. The median grain size of three of the deeper samples fall outside this range (see Table 7, Table 8 and Figure 19). The mud content (clay and silt fractions, <63 μm) of the surficial sediments ranges between 0 and 10%, although, if excluding sample BX6 of 10%, then all values are between 0 and 6.5%. For the deeper samples, mud content may be larger, reaching 50.4% for sample 11B. Samples BX6 and BX6B are less muddy than expected from the box coring onboard.

Commonly used measures for sorting are the d60/d10 or d90/d10 ratios, which for all surficial samples is small (well-sorted) and for some of the deeper samples much larger (poorly-sorted). With the grain-size distributions in this project, the 90-percent grain sizes have a larger range among samples, and therefore amplify the difference a little.

sample No.	< 63	d10	d50	d60	d90	d60/d10	d90/d10
BX01	4.69	93.04	219.82	262.43	569.85	2.82	6.12
BX02	4.55	94.58	198.85	229.51	413.65	2.43	4.37
BX03	2.73	181.43	431.43	501.22	893.70	2.76	4.93
BX04	0.00	183.24	285.84	313.14	446.31	1.71	2.44
BX05	1.85	158.84	408.80	478.20	860.80	3.01	5.42
BX06	10.03	61.78	162.41	181.30	272.82	2.93	4.42
BX06_B	20.31	8.84	158.20	179.01	274.92	20.25	31.09
BX07	3.67	123.70	239.50	272.46	464.18	2.20	3.75
BX08	3.68	113.32	262.26	310.32	615.91	2.74	5.43
BX08_B	0.25	429.27	806.28	910.87	1421.67	2.12	3.31
BX09	0.00	184.50	262.35	281.78	373.06	1.53	2.02

BX10	0.00	203.05	300.31	325.15	442.92	1.60	2.18
BX11	6.54	77.93	157.88	178.69	282.30	2.29	3.62
BX11_B	50.40	4.22	61.83	91.72	231.02	21.72	54.70
BX12	3.52	127.72	320.67	378.56	733.47	2.96	5.74
BX12_B	2.59	158.80	380.75	456.88	997.57	2.88	6.28
BX13	0.00	198.53	275.76	294.67	382.79	1.48	1.93
BX14	4.46	104.38	268.35	329.97	833.17	3.16	7.98
BX14_B	2.31	245.80	742.78	862.49	1416.23	3.51	5.76
BX15	3.15	119.36	286.92	335.89	591.41	2.81	4.95
BX16	2.18	195.68	334.14	370.82	549.93	1.90	2.81
BX17	3.76	113.22	195.92	216.98	319.67	1.92	2.82
BX18	5.24	138.83	298.73	339.66	538.87	2.45	3.88
BX19	2.77	154.04	361.05	420.88	770.49	2.73	5.00
BX20	1.91	195.14	330.40	366.46	543.28	1.88	2.78
BX21	0.00	178.41	262.84	284.57	389.06	1.59	2.18

Table 7: Grain-size characteristics of all samples, as calculated from the grain-size distributions with Malvern analyses. The _B numbers are the samples at depth; the other samples are surficial sediments (0 – 1 cm; or 0 - 2 cm where required).

One observation from these grain-size results (Table 7) is that sample BX10, with the thin mud drape, contains 0.00% mud in the analyses, and that BX1 contains mud in the analyses, but has no visible mud in the core and no mud drape on top. Also, BX1 is less well sorted than the other samples of the surrounding seabed, whereas in the gravel analyses (sieving) of the larger samples it is BX10 that contains more gravel. This suggests that the samples might have been swopped accidently in the lab.

	d50 (μm)	**%mud (vol%)**	**d60/d10 (-)**
MIN (surficial)	157.88	0.00	3.16
AV (surficial)	279.25	3.08	2.33
MAX (surficial)	431.43	10.03	3.16
MIN (all)	61.83	0.00	1.48
AV (all)	308.23	5.41	3.82
MAX (all)	806.28	50.40	21.72

Table 8: Overview of grain-size characteristics of the samples, separated for the surficial sediments and all samples: volume-percent of the mud fraction < 63 μm (%mud); median grain size (d50) and sediment sorting (d60/d10).

The cumulative grain-size distributions in Figure 19 display the well-sorted nature of the surficial sediments. The colour-coding indicates different types of locations and zones of contrasting backscatter (see figure caption). The samples from the 'original' sea bed surrounding the MV2 North and South sand pits (red curves), are the best sorted sediments.

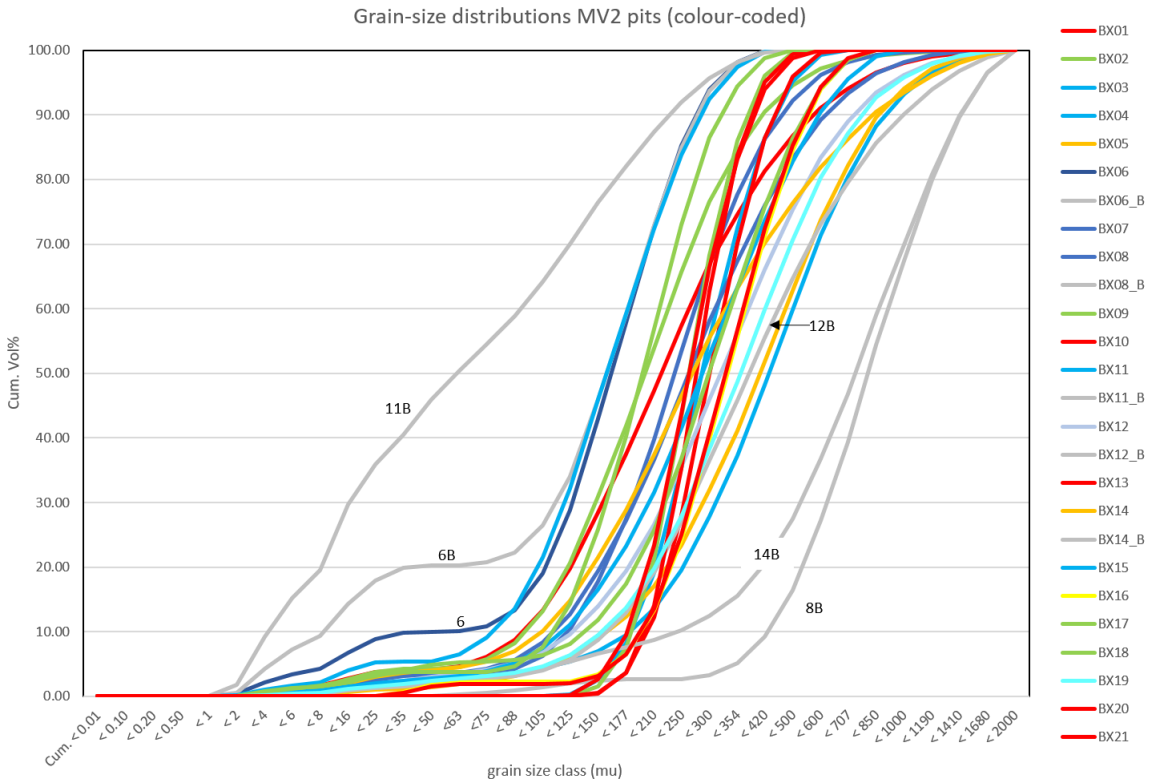

Figure 19: Cumulative grain-size distributions of the fractions smaller than 2 mm (Malvern analyses) of all samples (including the B-samples at depth). The colour-coding indicates the type of location and areas of contrasting backscatter: surrounding sea bed (red), bottom of sand pit (blue shades), slopes of sand pits (green), area of high backscatter (orange), area of lower backscatter identified to contrast with high BS (yellow) and samples at depth (light grey and labelled). These cumulative grain-size distributions show that all surficial sediments are well- to moderately well-sorted (steep curves), but that the deeper samples of BX6_B and 11_B are poorly sorted. Samples BX6 and 6B are less muddy than expected from the coring onboard; despite the 10% and 20% mud content, respectively, these samples still contain a large amount of very fine to medium fine sand. BX8_B and 14_B are well-sorted, but considerably coarser than the other cores.

The median grain size and sorting characteristics of all samples are also displayed in the colour-coded bivariate plot below (Figure 20). This is merely a different way of illustrating the earlier finding: all surface sediments are well- to moderately well sorted. Only 6_B and 11_B at depth are poorly sorted (these are the fine-grained deposits with high mud contents). BX8_B and 14_B are similarly well-sorted, but have a much coarser median grain size (these are the Kreftenheije deposits).

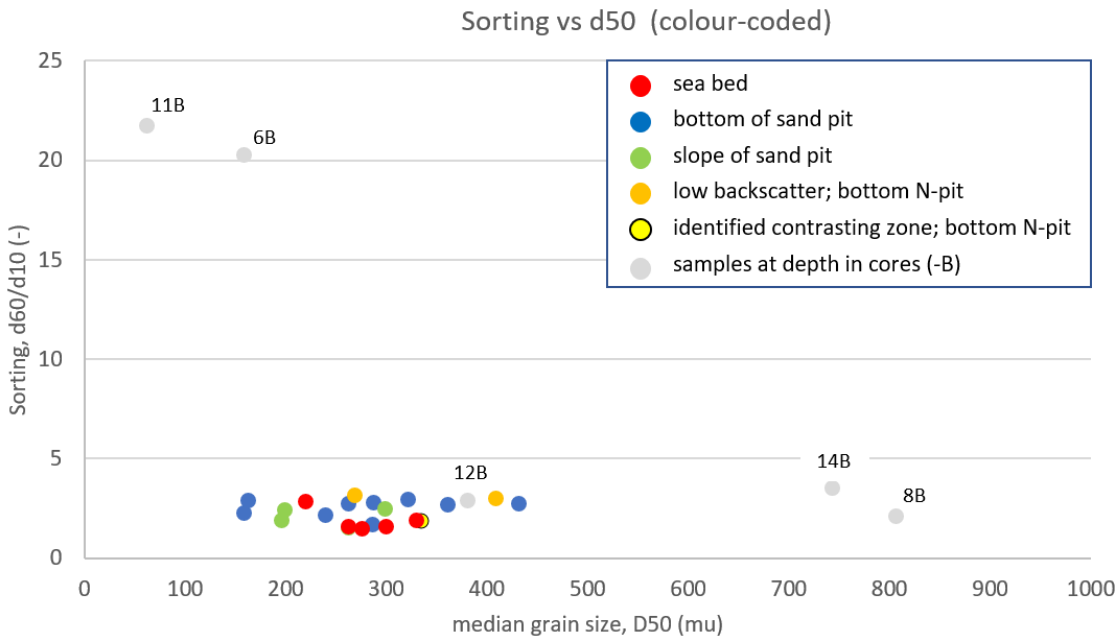

Figure 20: Grain-size sorting (d60/d10) versus median grain size (d50) of all samples, with similar colour coding as in Figure 19. All samples at the bed surface (0-1 and 0-2 cm) are clustered in a narrow group of similar sorting with a d50 ranging from 160 to 430 μm. The four samples that are in sharp contrast with the main group are samples at depth: 11B and 6B (fine-grained and poorly-sorted) and 14B and 8B (similarly well-sorted as the majority of the samples, but very coarse: these two samples were identified to be of the Kreftenheije Formation).

Just to determine whether the sediments from the North-pit and South-pit show contrasting sediment grain-size characteristics, geographically, Figure 21 plots the sorting vs. d50, separately for samples in or around the North-pit (BX1 – 16) and those in or around the South-pit (BX17 – 21). The two areas occur in the same point cloud, so samples do not geographically differ.

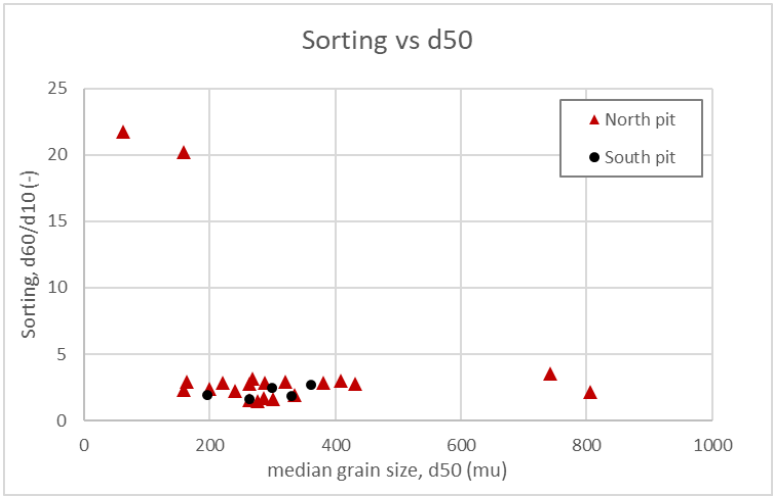

Figure 21: Grain-size sorting (d60/d10) versus median grain size (d50) of all samples, showing that the sediment characteristics do not geographically differ.

3.4.2 Gravel fraction

Of the larger samples that were sieved, particularly BX12 and BX16 contained coarse material, including whole dead sea urchin crusts, whole shells (gastropods, half bivalves), and siliclastic and carbonate fine gravel (Figure 22). Grain-size distributions of the mud, sand and gravel fractions combined are displayed in Figure 23. The mismatch between curves is because these

result from separate analyses. The analyses of the mud-sand fractions were all within the accuracy requirement of less than 0.4 g difference.

Figure 22: Photos of coarse material on the sieves. Left: BX12, old Ensis sp. on 16-mm mesh and half bivalves on the 8- and 4-mm meshes. Middle: BX16, dead sea urchin crusts on a 16-mm mesh, gastropods on the 10-mm mesh and half bivalves on the 8- and 4-mm meshes. Right: BX16, 2-mm sieve with fine gravel and shell/urchin fragments (carbonate gravel).

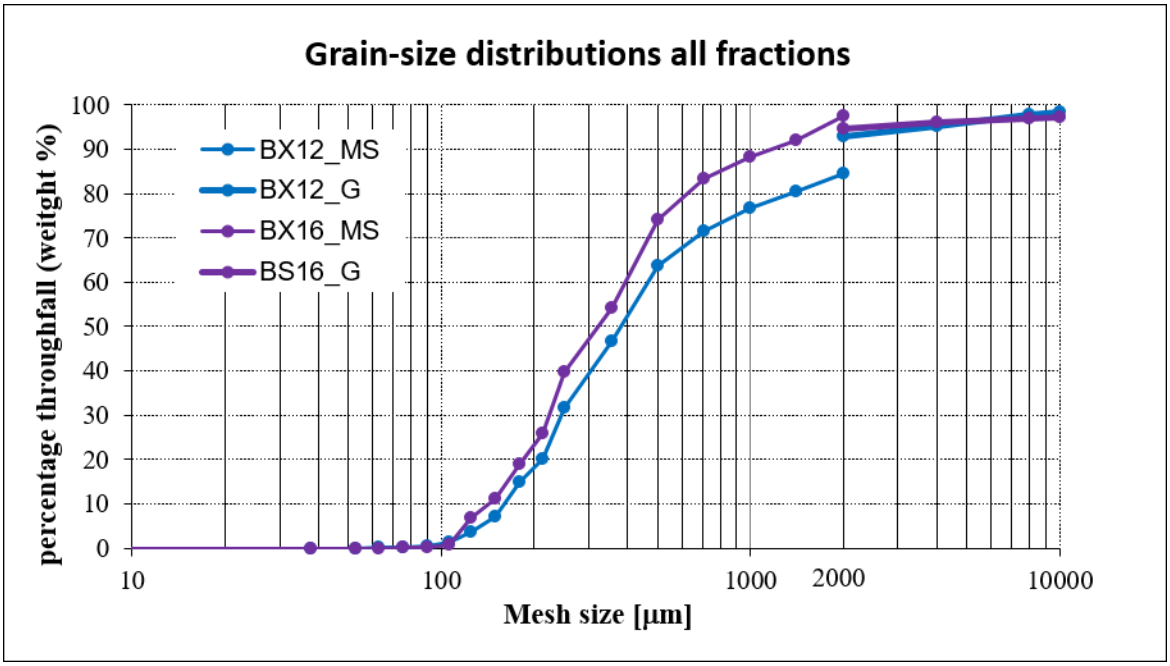

Figure 23: Cumulative grain-size distributions of all fractions for BX12 and 16 (_MS, mud-sand; _G, gravel). The curves do not match, because sieving was conducted in two separate analyses (<2000 µm and >2000 µm).

Data of the grain-size analyses by both Malvern and sieving are provided with this report in Excel sheets (Products\Malvern results.xls and \Sieving results.xls).

3.4.3 Folk classification

All surface samples are classified as slightly gravelly sand, (g)S, based on the Malvern grain size results and the Folk classification for the gravel-sand-mud fractions, thus including the residues of > 2 mm (i.e. each sample contained more than a trace (0.01%) of gravel). The full fractions are also what the acoustic signal measured at the seabed. If we would have classified the samples of the < 2 mm only (Malvern analyses), then all samples would classify as Sand (S), since all samples contain more than 90% of sand. BX6 is the only sample – of the 0-1 cm surface samples – that contains 10.03% mud, which places it directly on the line between slightly gravelly sand, (g)S, and slightly gravelly muddy sand, (g)mS, but only just.

Of the deeper samples, only two samples show a different class: 6B is (g)mS and 11B is (g)M (slightly gravelly mud). Three out of five deeper samples (8B, 12B and 14B) are (g)S, similar to the surface samples. The Folk classes per box core are listed in the grain size results table (Excel file appended to this report).

We have not classified the sediment distributions resulting from the sieving, since, of the surficial samples, only BX12 has a gravel content of larger than 5%, which would classify as gravelly sand (gS) instead of slightly gravelly sand ((g)S).

3.5 Ground truthing for sediment mapping of sand extraction pit MV2

For high-resolution sediment mapping, using bed classification of multibeam backscatter data, sediment characteristics are assigned to the acoustic bed classes (ASC's in Figure 14), as ground truthing. Correlation plots of ASCs and sediment characteristics here used (median grain size, mud content, and sediment sorting, d60/d10 and d90/d10, from Malvern analyses (<2 mm fractions)) display the correlations (Figure 24). In the interpretation of the correlation plots, we compared the results from bed classifications with 3, 4, and 5 classes. In the bed classification with 3 classes, ASC1 is represented by all samples from the surrounding seabed (BX1, 10, 13, 20 and 21) plus BX9 and BX16, which in the core descriptions were identified to be most similar to the seabed samples and displayed grain-size distribution curves that were nearly identical to the seabed samples (BX16 ≈ BX20 and BX9 ≈ BX21, see section 3.4) When comparing the 4-classes bed classification results to the 3-classes results, BX9 and 13 are separated into the extra class of lower backscatter (ASC1); all other classes (now 2, 3 and 4) remained unchanged. ASC1 and 2 are thus a very robust class when comparing it to the sediment cores and correspond to the observed backscatter strengths in the backscatter mosaic (Figure 13). ASC3 comprises BX3, 6, 7, 11, 15, 17, 18, spanning from fine-grained cores (6 and 11) to the large d50/low mud% of BX3. Class 4 comprises BX2, 4, 5, 8, 12, 14, 19, thus – indeed – including the two BX-samples that were selected for high BS (BX5 and 14) and the coarser deposits of BX5 and the two Kreftenheije deposits (BX8 and 14).

With the ASCs based on backscatter strengths measured during the survey and the relation between backscatter and sediment characteristics, ideally, the correlations would show a clear correlation and little overlap in the sediment characteristics among ASCs. For the bed classification with 4 classes, here presented, the overlap among ASCs for the median grain size, d50, is large (Figure 24, top chart). For mud content (%mud, one chart lower), ASCs 1 to 3 show increasing values, but class 4 shows a lower mud content, and the samples without any mud (0%) occur in 3 bed classes.

For sediment sorting, where the d90/d10 amplifies the difference among samples when compared to d60/d10, a fair correlation is exhibited in the plots (Figure 24, lower two charts) with little overlap among the ASCs. The more, when the "outliers" (samples BX1 in ASC2 and BX4 in ASC4) are neglected, although it must be said that the number of box cores taken is too small to statistically identify outliers. Nevertheless, if BX1 was indeed accidently swopped in the lab (which is suspected) with BX10, then the high mud content of this outlier is due to the

thin mud veneer at the surface of BX10. This would suggest that the thin mud drape does not significantly affect the BS strength: the seabed sample still classifies in the same ASC comprising all samples of the surrounding seabed. For discussion on this, see Chapter 4.

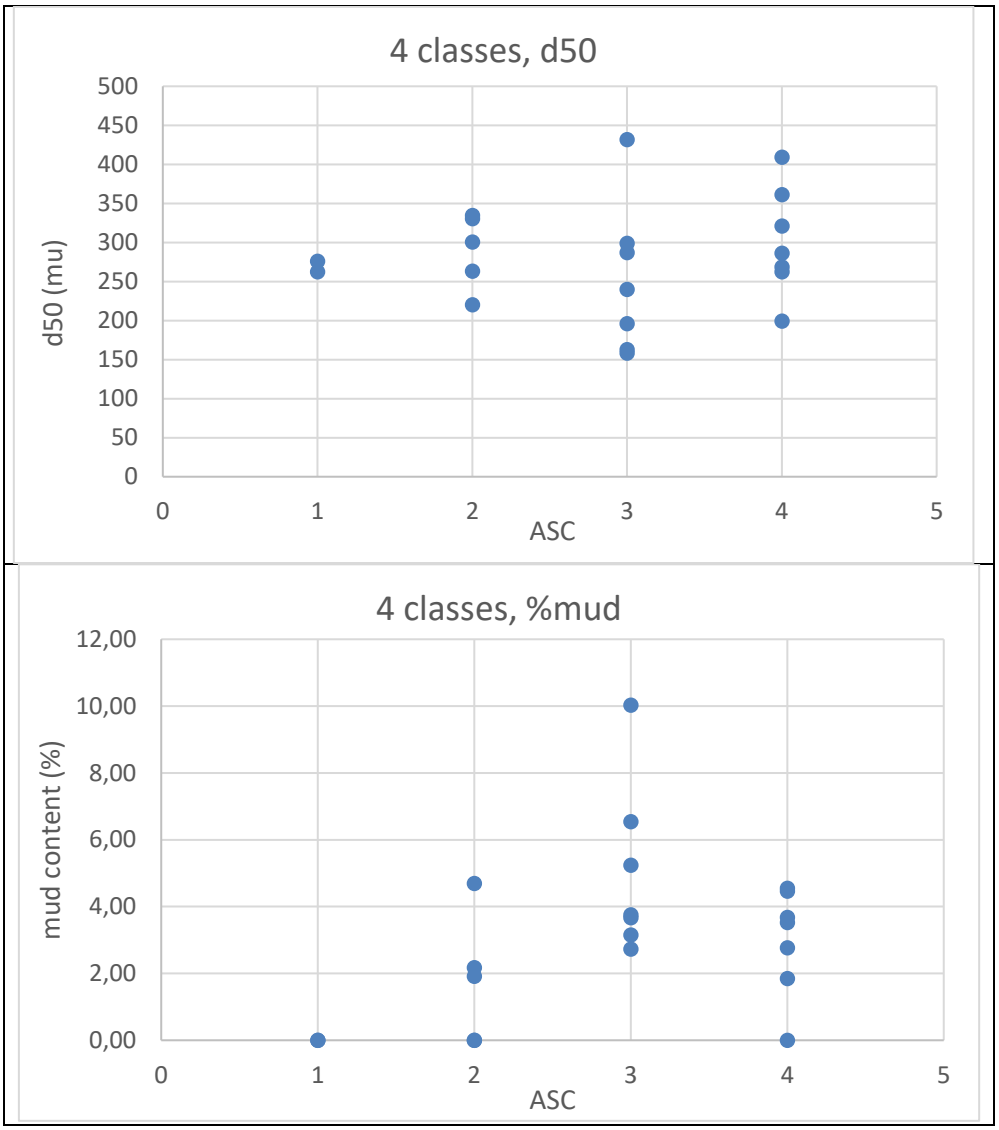

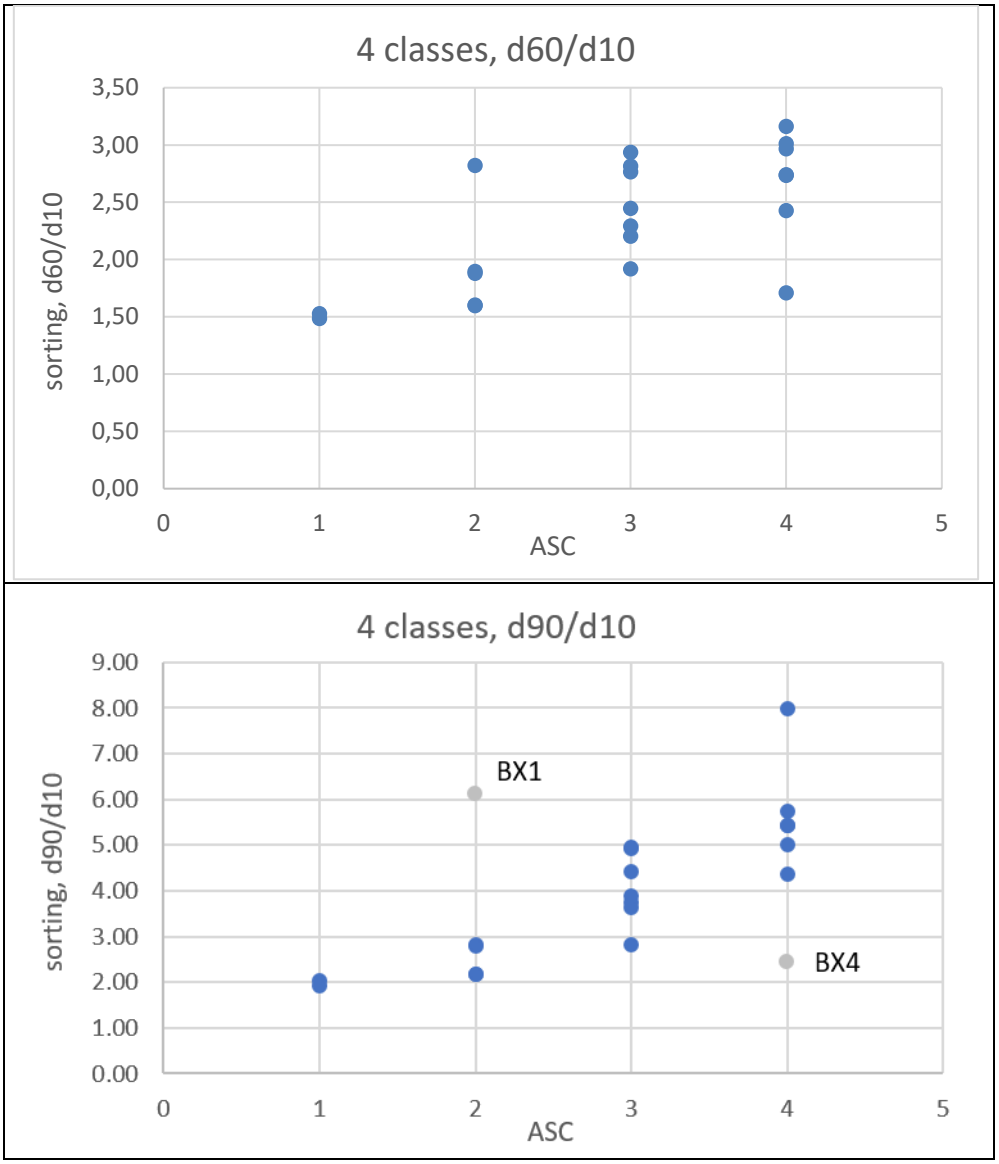

Figure 24: Correlation plots of acoustic class (ASC) and sediment characteristics, from top to bottom: median grain size (d50), mud content (%mud) and sorting (d60/d10 and d90/d10) for surface samples only, as determined in the Malvern analyses (< 2000 mu fractions) and averaged ASC extracted from the ASC map at BX locations with a 2-m radius. Class 1: BX9, 13; Class 2: BX1, 10, 16, 20, 21; Class 3: BX3, 6, 7, 11, 15, 17, 18; Class 4: 2, 4, 5, 8, 12, 14, 19.

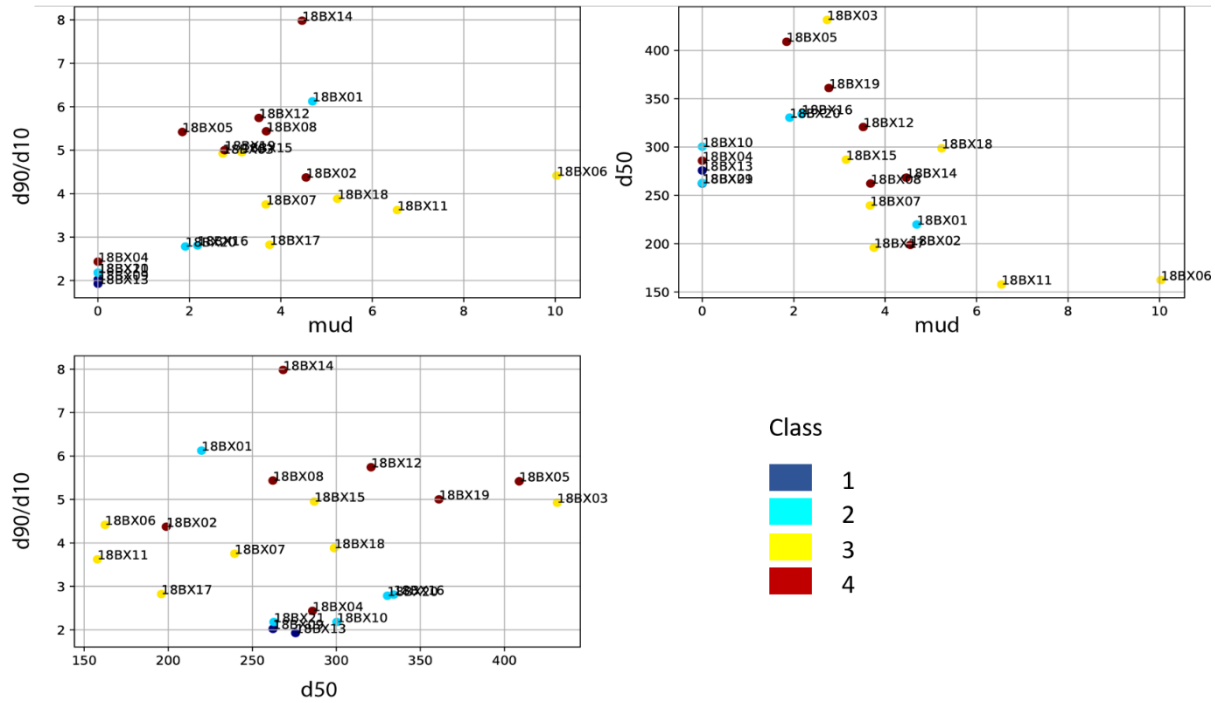

Figure 25: Bivariate plots of two grain size characteristics on the axes and colour-coded ASCs. Top left: d90/d10 vs. %mud; top right: d50 vs. %mud; bottom left: d90/d10 vs d50.Clustering of the classes (colours) reveals a good discrimination of sediment characteristics among the ASCs.

Furthermore, we plotted bivariate plots of two sediment characteristics and colour-coded the ASCs (Figure 25). For all three combinations (sorting/%mud; d50/%mud; sorting/d50) there is a reasonable clustering of the ASCs (colours): ASC1 (navy) at the lower ends of plots, ASC2 (light blue) just above that (except for outlier BX1, which may be BX10 with mud veneer), ASC3 (yellow) is separated from ASC4 in the two plots that include sorting. In the clustering, only BX 1, 2 and 4 are off. So for BX1 (BX10) the exception is the mud veneer, for BX2 and BX4 are no sedimentological observations that would label these as outliers. These plots too, visualise that the range of median grain size is large within classes (ASC3 and 4) and that sorting distinguishes the samples best.

Following the recent literature on the Bayesian sediment classification, in which Folk classes of sediment type are assigned to the acoustic classes, in case of the MV2 pit measurements, the correlation would have all four ASCs on one line of sediment class (g)S (full overlap). This would mean that the MBES-backscatter measurements are able to pick up more subtle differences in sediments in the field than is represented by the differentiation in the Folk classification.

3.6 Resulting seabed sediment-classification map

Based on the observations of assigning surface samples of box cores to ASCs as ground truthing, the acoustic bed classes may represent the following sediment types (Table 9):

ASC1 *lowest BS*	Well-sorted, slightly gravelly, medium coarse sand with 0 to extremely small mud content	Surrounding seabed and slope N-pit
ASC2 *low BS*	Well- to moderately sorted, slightly gravelly, 0 to slightly silty, medium to very coarse sand, with a trace of to few shells	Surrounding seabed and slope N-pit
ASC3 *medium BS*	Moderately sorted, slightly gravelly, slightly to moderately silty, medium fine to extremely coarse sand with a trace of to few shells	Bottom and slope of sandpits
ASC4 highest BS	Moderately sorted, slightly gravelly, 0 to slightly silty, medium fine to very coarse sand with a trace to few shells	Bottom and slope of sandpits

Table 9: Interpretation of acoustic classes (ASCs) for sediment mapping, after ground truthing with sediment characteristics, as analysed form sediment cores (box cores)

The differences in sediment characteristics among classes (Table 9) are extremely subtle and can hardly to not be told apart from sedimentary descriptions, and yet the acoustic backscatter values identify different zones. Descriptive sediment classifications, such as NEN and Folk, therewith seem too general to label the bed classification from high-resolution backscatter measurements (this was also found by Koop et al., 2019). In Table 9, the larger silt content (ASC3) and larger range in median grain size (ASCs 3 and 4), both resulting in poorer sorting, distinguish between acoustic classes 1 and 2 on the one hand, and classes 3 and 4 on the other. The difference between class 3 and 4 is hard to tell from the descriptions, but the bottom correlation plot in Figure 24 reveals that ASC4 comprises the poorest sorting.

The resulting sediment map, based on the Bayesian acoustic bed classification, using MBES backscatter measurements, is presented in Figure 26.

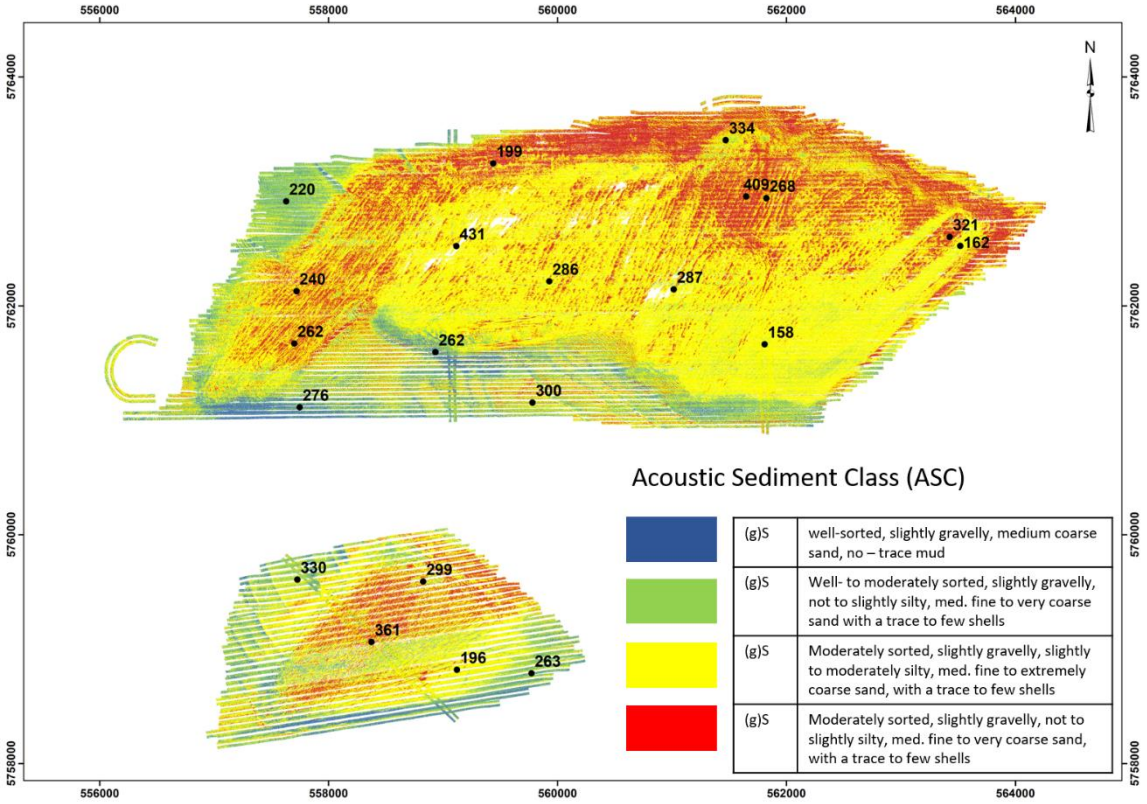

Figure 26: Resulting sediment map of the Maaskvlakte 2 sand extraction pits and surrounding seabed. Co-ordinates are in UTM31N ETRS89.

Notwithstanding the subtle differences in the parameters of grain size distributions so far examined in this study of surficial sediments, the MBES backscatter measurements distinguish 3 to 8 classes. Therefore, it is likely that also other (sedimentary) characteristics of the bed may add to the varying backscatter strengths that discriminate seabed sediment in different acoustics classes. More sediment and bed characteristics are examined in Chapter 4 Discussion.

4 Discussion

The in this report presented results are based on choices in the bed classification method and ground truthing in a – what turned out to be a – relatively homogeneous area (in terms of grain-size characteristics). The Bayes bed classification method here applied, uses a selection of beams and objectively calculates the optimal number of classes in the bed classification of backscatter measurements, corrected for transmission losses and bathymetry. These choices are partly subjective and will be discussed below. Also, few other sources of uncertainty in the measured backscatter are not - or cannot be at this time - corrected for (e.g. the effect of suspended matter in the water column).

4.1 Choices in and interpretation of the acoustic bed classification method

Selection of beams
Backscatter data around nadir (mostly 0 – 10 degrees) are prone to specular reflection and are therefore too noisy to provide a reliable classification and the backscatter of the outer beams is more discriminative (Gaida et al., 2018b; Snellen et al., 2019). In the recent literature on the Bayesian bed classification method, Gaida et al. (2018a) used and compared selected beams, e.g. 48° and 54°, and Gaida et al. (2018b) used a range of 40 – 60° beams for the backscatter analyses. In this study, we used the 54, 56 and 58° beam angles as reference angles and did the analyses over the 20 – 64 degrees beams. Figure 7 reveals that the shape of the backscatter histograms significantly differ for different beams, and, although the performance of the approximation of the measured backscatter histograms was tested on a large number of beams, ranging from 37 to 64° (Figure 8), additional testing is needed for corroborating the choice of beam angles made in the bed classification.

Number of classes in Bayes bed classification
The number of acoustic sediment classes recommended by the method for the tested beam angles, varied between 3 and 8 ASCs. This is a more ambiguous result than was to be expected, based on the method results in the literature. For finding out what number of classes would be optimal, a closer inspection of the outliers (in number of classes) should be performed. The approximations of the corrected backscatter histograms calculate that three ASCs is the least number of classes for an adequate fit. In Figure 8, the plots with 3 classes show Gaussians with little overlap and thus distinguishable classes. Plots with more than 4 classes, however, show fully overlapping Gaussians, which in practice, becomes more difficult to interpret. Here we chose for 4 bed classes, based on the principle to opt for the least number of classes. The improvement of the bed classification is only little when increasing the number of ASCs to 5, 6, 7 or 8 classes, and with fully overlapping Gaussians, a larger number of classes could be overinterpretation of the data. The sediments in the MV2 sandpit area, vary only little in grainsize, whereas the datasets in the recent literature comprise the full range of Folk classes, from sandy mud to sandy gravel (Gaida et al., 2018a; 2018b; Snellen et al., 2019).

The acoustic classes in this study, partly correspond to the different environments, with ASC 1 and 2 mostly representing the surrounding seabed and ASC 3 and 4 representing the sandpits' floors and slopes. An extra test for the optimisation of the bed classification results would be performing the bed classification separately for the different environments.

Other factors that may affect the backscatter measurements may be, for example, suspended sediment concentrations in the in the water column, which are not considered in this pilot. The

effect of suspended sediment is still a subject of ongoing research in the scientific literature. During our survey, however, the 0 g/l sediment concentration in the water samples near the bed and the very thin drapes in the box cores after a fair-weather period and the theoretically low hydrodynamics (current and waves) in the sandpits, imply that suspended sediment may not be affecting the backscatter data in this study.

4.2 Ground truthing

The correlation and bivariate plots presented in section 3.5, show that only BX1, BX2 and BX4 cause a slightly ambiguous result in the assignment of sediments to ASCs. If BX1 was indeed swopped with BX10, then it is the mud veneer at the surface which makes that this point is an outlier. Grain-size characteristics of BX2 and 4, however, are not extraordinary. Other factors that could cause changes in backscatter strengths are *(i)* biology, such as alive macrobenthos on the seabed, protruding from the bed or directly below the surface, *(ii)* the presence of siliclastic or carbonate gravel (grains or shells), *(iii)* mud veneers, fluid mud, or underlying layers of contrasting sediments within the depths that are affected by acoustic scattering, or *(iv)* bed roughness of the resolution of the backscatter.

The classification of BX1 (BX10) in ASC2, the class that represents the surrounding seabed, together with the bare-sand surfaces, as well as the samples with mud veneers in ASC3, suggest that the mud veneer does not significantly affect the backscatter measurements. The effect of thin drapes of mud – as well as fluid mud – is still under debate in the scientific literature. In a study on benthic habitat mapping, using bed classification based on side-scan sonar backscatter, Van Dijk et al. (2012) reported thin mud veneers in the swales of the tidal ridge Brown Bank on the Netherlands Continental Shelf and speculated on the effect on diagnostic acoustic facies. Koop et al. (2019) applied the Bayes bed classification method in the Brown Bank area, but used grab samples (which mix sediments and obscure sediment layering) for sediment grain-size distributions and, although they also use video footage, the influence of mud drapes on backscatter was not established. In previous studies, mud layers (mud as main lithological fraction) have been identified in acoustic bed classification (Gaida et al., 2018b; Snellen et al., 2019 and references therein). At this time, it remains unknown how thick mud layers need to be for identification as a different sediment class in the seabed sediment classification using MBES backscatter measurements. Or, how thin the overlying sandy layer may be for obscuring clay layers in the subsurface. A possible way to gain more insight in the effect of mud or sand covers and their thicknesses, might be multi-frequency multibeam: Gaida et al. (2018b) report on the differential penetration in mud and sand layers and the detection of different layers in the shallow subsurface.

Sample BX2 had a high density of protruding tube worms, which also occurred in samples BX5 (Figure 27a) and in lower density in a few other cores.

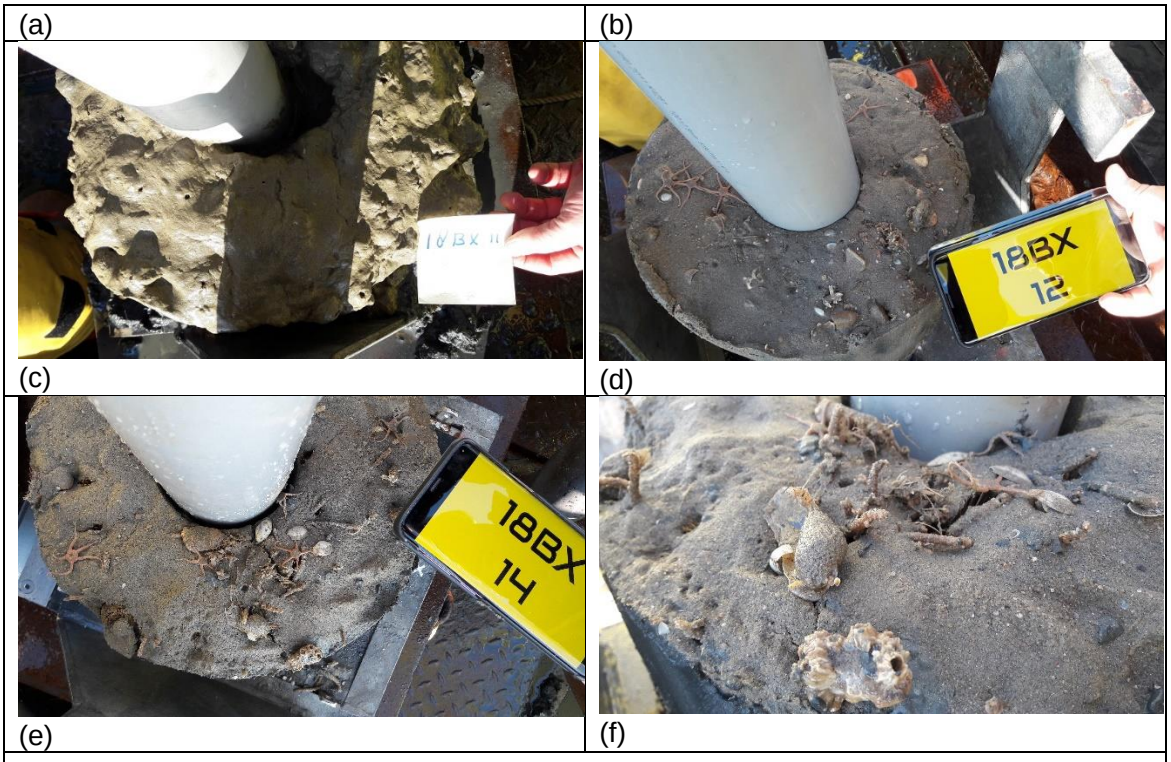

Figure 27: Examples of different seabed surfaces: (a) protruding tube worms BX5, (b) bare-sand surface BX13, (c) the muddy surface of BX11 is bumpy, entirely crammed with small (juvenile?) sea urchins, (d) gravel, some shells and snake stars on BX12; (e) shells, snake stars and hermit crabs and barnacles on BX14, and (f) closeup of BX14.

Box cores 6 and 11 are much finer-grained than the other samples, but still are in ASC3, possibly related to a sandier surface layer. The bumpiness of BX11 due to high density of small (juvenile?) sea urchins within the top 2 cm of the surface (Figure 27c) may affect the acoustic backscatter.
There is no indication that the coarse Kreftenheije deposits at 6 – 8 cm depth in BX8 and BX14 have an effect on the backscatter. It is more likely that the seabed with alive and dead benthos influences the backscatter. Using a multi-frequency multibeam would be useful in this case: the lower frequencies have a higher penetration into the subsurface and the comparison of backscatter data at different frequencies might allow for the detection of sedimentary layers in the very shallow subsurface (Gaida et al., 2018b).

Gravel content
The backscatter response on coarser sediments, like gravel, may be ambiguous. Where it is thought that the backscatter strength increases with grain size, for the coarser sediments, the backscatter may be decreasing again (e.g. Gaida et al., 2018a). A correlation plot of the gravel fraction as residues from the Malvern analyses (Figure 28a), shows large overlap among ASCs, similar to the d50 in section 3.5. Because those residues from the Malvern analyses are not statistically representative for amounts of gravel, we consider the sieving results of the larger samples (taken for the purpose of determining gravel content). The fair correlation in these plots (Figure 28b and c), of increasing gravel content with ASCs, suggests that gravel content may be a discriminative factor for MBES backscatter strengths.

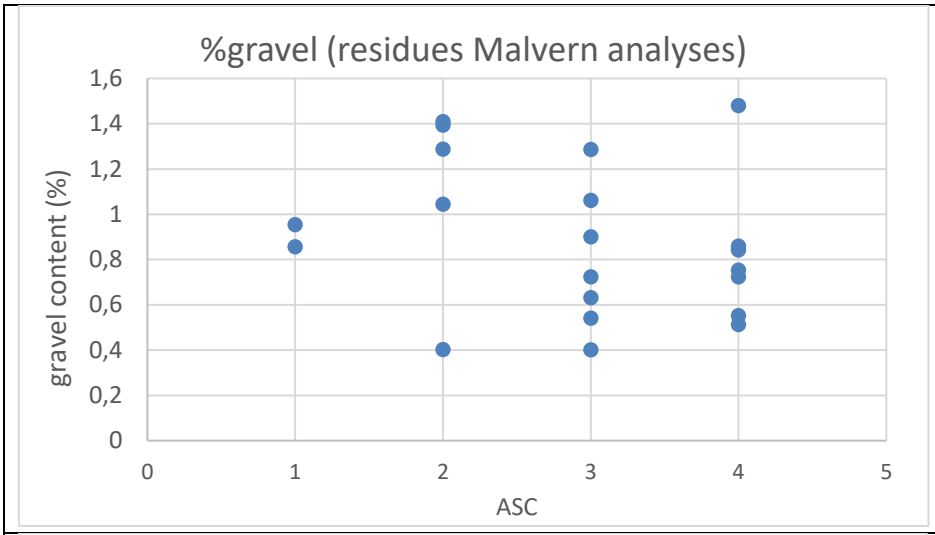

(a)

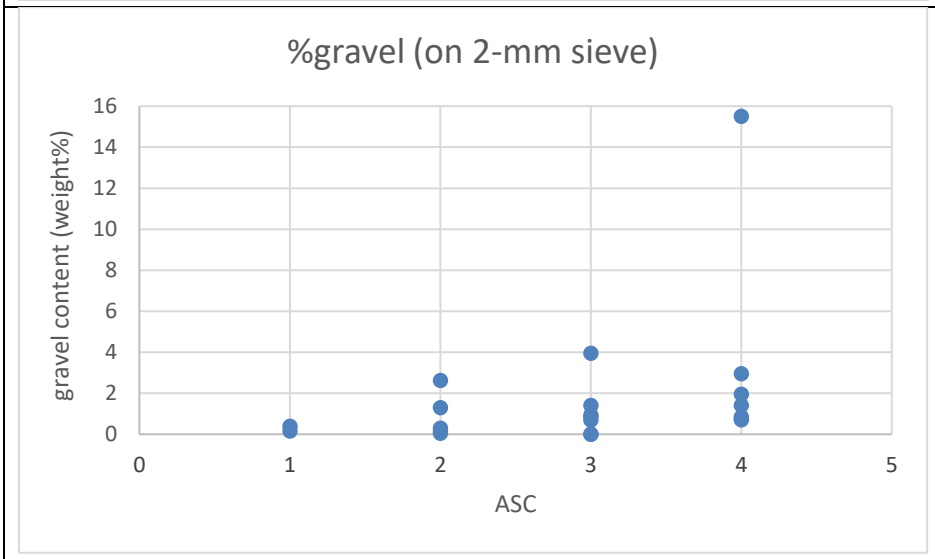

(b)

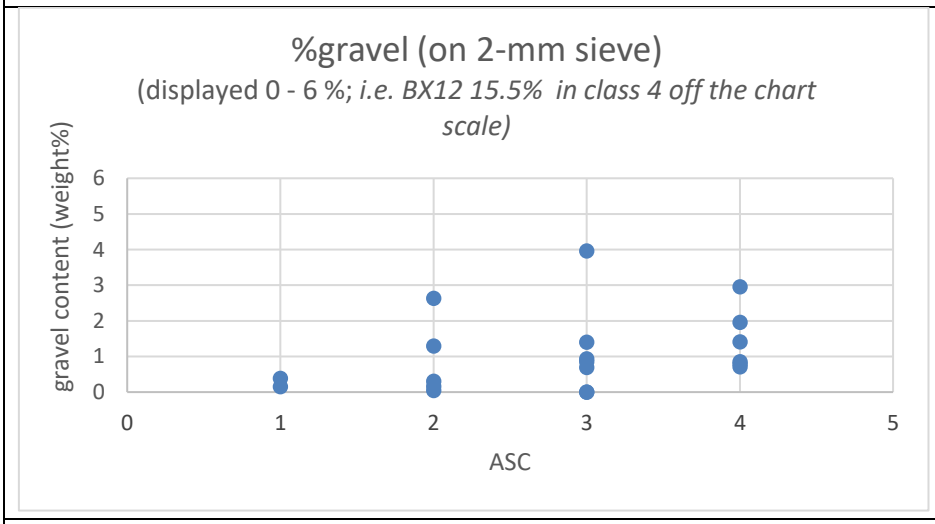

(c)

Figure 28: gravel content from (a) the residues of the Malvern analyses (not statistically valid), (b) from the sieving analyses of the sand and mud fractions (remainder on the 2-mm sieve), and (c) idem (b) but displayed on a smaller range (BX15 not visible). The sieving results show a fair correlation of increasing gravel content with ASC.

Despite the subtle variation in sediment types that occur in the study area (one Folk class, narrow range of grain-size distributions and core characteristics), the MBES backscatter measurements revealed distinct differences in backscatter strengths after correction for transmission losses and sea bed morphology (grey tones in Figure 13), leading to four classes in the bed classification, thereby separating sediments of different grain-size distributions, in which especially sorting and gravel content seem to be discriminative. The backscatter patterns are believed to validly represent sediment properties in the study area. Although interpretation still needs more thorough investigation of the results, the finding that the MBES backscatter measurements are able to pick up subtle differences (too subtle for Folk classifications) thus demonstrates the great advantage of the acoustic bed classification in high-resolution sediment mapping: in the classical way, using box cores only, the map of the MV2 pit areas and surrounding seabed would have been one sedimentological unit, (g)S, whereas with the acoustic measurements, areas can be distinguished based on their contrasting backscatter strengths from area-covering measurements.

In the 21 sediment cores, mud layers are only present in BX6 and BX11 the north-eastern and eastern part of the North-pit, respectively, and not in the rest of the North-pit and South-pit. BX6 penetrated the full length of the box corer, but did not reach the bottom of this mud layer. So in the dredging trench, the mud layer is more than 60 cm thick. BX11 revealed a slightly silty sand deposit below the clay layers at 12 cm, which may be the top of the sediments underlying the mud layer (then the mud layer is 12 cm thick here). Water samples near the bed were clear (SSC = 0%) and, even after period of fair weather, mud drapes at the surface were only very thin (<<1 to 1 mm); they also only occur in a small number of box cores, and not only in the pit, also in the surrounding seabed. These thin, surficial drapes are interpreted as natural tidal deposits; the absence of tidal mud drapes in the sandy cores (at depth) implies that – at the surrounding seabed – these may be temporary drapes that may be removed again at times of more energetic hydrodynamics and/or – in the pit – may be mixed in the top layers by bioturbation. Therefore, observations do not give a reason to believe that the pit is being filled in with mud in a significant rate. However, the area in which the fine-grained box cores BX6 and BX11 occur, is represented by acoustic class 3 in the bed classification map, based on 4 classes (yellow in Figure 26). This area, of purely class 3, is located in the part of the North-pit that was abandoned for dredging first, which is also the deepest part of the pit. That could mean that in other parts of the pit, which are more recently abandoned or still being actively used for dredging, fine-grained sediments may settle later. The distribution of the coarser sands is geological, with the Kreftenheije deposits in some of the elevated parts of the North-pit.

5 Conclusions

Sediments in the seabed surrounding the MV2 sand extraction pits comprise well-sorted, slightly gravelly sands ((g)S). Sediments in the sand pits are well- to moderately sorted, slightly gravelly, slightly silty sands (all (g)S), with in the shallower northern and western parts of the North-pit coarser deposits of the Kreftenheije Formation. Only in a dredging trench and the eastern part of the North-pit, fine-grained muddier deposits were observed. Median grain sizes of all surficial samples range from 157 to 431 μm. There is no indication that the sand pits are being filled in with mud at a significant rate, neither from box core characteristics and grain-size analyses (locally thin mud veneers) nor from the sediment classification map (Figure 26).

Despite the subtle variation in sediment characteristics in the study area, the Bayes bed classification method, using high-resolution MBES backscatter measurements, is able to pick up variations in backscatter strengths and distinguishes four acoustic sediment classes. This demonstrates the great advantage of high-resolution MBES backscatter measurements compared to the classical sediment mapping method (based on sampling only and interpolation), where the mapping of the study area would have resulted in a map with one unit, slightly gravelly sand, throughout the area. The MBES backscatter method thus picks up more subtle classes than the Folk sediment classification and tremendously enhances the seabed sediment mapping, not only in resolution (raising the resolution by a factor of hundreds) based on real observations, but also in discrimination power and identification of sediment types. Furthermore, MBES backscatter measurements are acquired simultaneously with MBES bathymetry measurements, and thus is an efficient and cost-effective mapping method, not requiring additional surveying time.

The results presented in this report are a pilot to test the performance of the bed classification method in sandy areas of the Netherlands Continental Shelf and to map the seabed sediments in the Maasvlakte 2 sand extraction pits. Further investigation needs to be done on the choices that need to be made in the method and their effects, in order to improve the interpretation of sediment mapping using MBES backscatter data and to specify what characteristics of sediment are discriminative in backscatter data in – sedimentologically – relatively homogeneous sea beds.

Sedimentary interpretation using bed classification based on high-resolution MBES-backscatter data provides insight in the quality of the sediments in terms of sand as a resource for industrial purposes and is a valuable tool for abiotic properties of the seabed for habitat mapping in ecological studies, such as monitoring programmes for recolonisation of benthic fauna in anthropogenically influenced areas.

6 Acknowledgements

This project was possible thanks to Ad Stolk, Rijkswaterstaat Zee en Delta, who valuably contributed to all parts of the project and organised the availability of the RV Arca of Rijkswaterstaat. 24-Hour surveying by the RV Arca crew allowed for being able to collect all data within 4 days, including the box cores. The team of project guests on board during the survey comprised of Ad Stolk (RWS-ZD), Timo Gaida (Delft University of Technology), Marios Karaoulis (Deltares) and Thaiënne van Dijk (Deltares). Timo Gaida led the survey on board, so that the backscatter data in SIS were carried out successfully. Timo Gaida and Mirjam Snellen, Delft University of Technology, made the bed classification method available and transferred knowledge on the use and interpretation of the method. Deltares funded the knowledge exchange and development, dovetailing with this project, from the Strategic Research Programme ‘Subsurface resources in a circular economy’.

7 References

Amiri-Simkooei, A.R., Snellen, M. and Simons, D.G. (2009). Riverbed sediment classification using multi-beam echo-sounder backscatter data. J. Acoust. Soc. Am. 126: 1724–1738.

Brown, C.J., Smith, S.J., Lawton, P. and Anderson, J.T. (2011). Benthic habitat mapping: A review of progress towards improved understanding of the spatial ecology of the seafloor using acoustic techniques. Estuar. Coast. Shelf Sci. 92: 502–520.

Eleftherakis, D., Berger, L., Le Bouffant, N., Pacault, A., Augustin, J.M. and Lurton, X. (2018). Backscatter calibration of high-frequency multibeam echosounder using a reference single-beam system, on natural seafloor. Mar. Geophys. Res. 39: 55–73.

Folk, R.L. (1954). The distinction between grain size and mineral composition in sedimentary rock nomenclature. The Journal of Geology 62(4): 344-359. https://doi.org/10.1086/626171.

Gaida, T.C., Snellen, M., Van Dijk, T.A.G.P. and Simons, D.G. (2018). Geostatistical modelling of multibeam backscatter for full-coverage seabed sediment maps. In: S.J. Degraer, V. Van Lancker, S.N.R. Birchenough, H. Reiss & V. Stelzenmüller (Guest Eds.): Interdisciplinary research in support of marine management, Special Issue, North Sea Open Science Conference. Hydrobiologia, 1-25, https://doi.org/10.1007/s10750-018-3751-4.

Gaida, T.C., Tengku Ali, T.A., Snellen, M., Amiri-Simkooei, A., Van Dijk, T.A.G.P. and Simons, D.G. (2018b). A Multispectral Bayesian Classification Method for Increased Acoustic Discrimination of Seabed Sediments Using Multi-Frequency Multibeam Backscatter Data. In: M. Diesing and P. Feldens (Guest Eds.): Geological Seafloor Mapping, Special Issue, ISSN 2076-3263. Geosciences 8(12): 455-480; https://doi.org/10.3390/geosciences8120455.

IHO (1988). IHO Standards for Hydrographic Surveys. Monaco, International Hydrographic Bureau.

Jackson, D.R. and Richardson, M.D. (2007). High-Frequency Seafloor Acoustics. In High-Frequency Seafloor Acoustics, Springer: New York, NY, USA.

Koop, L., Amiri-Simkooei, A., Van der Reijden, K.J., OFlynn, S., Snellen, M. and Simons, D.G. (2019) Seafloor Classification in a Sand Wave Environment on the Dutch Continental Shelf Using Multibeam Echosounder Backscatter Data. Geosciences 9, 142, doi:10.3390/geosciences9030142.

Lecours, V., Dolan, M.F.J., Micallef, A. and Lucieer, V.L. (2016). A review of marine geomorphometry, the quantitative study of the seafloor. Hydrol. Earth Syst. Sci. 20: 3207–3244.

Lurton, X. (2010). An Introduction to Underwater Acoustics; Springer: Berlin/Heidelberg, Germany, 2010.

Lyons, A.P. and Abraham, D.A. (1999). Statistical characterization of high-frequency shallow-water seafloor backscatter. J. Acoust. Soc. Am. 106: 1307–1315.

Nguyen, T.K. (2017). Seafloor classification with a multi-swath multi-beam echo sounder. Signal and Image processing. Thesis, Ecole nationale supérieure Mines-Télécom Atlantique, 2017. English. ANNT: 2017IMTA0035.

Roche, M., Degrendele, K., Vrignaud, C., Loyer, S., Le Bas, T., Augustin, J.M. and Lurton, X. (2018). Control of the repeatability of high frequency multibeam echosounder backscatter by using natural reference areas. Mar. Geophys. Res. 39: 89–104.

Schimel, A.C.G., Beaudoin, J., Parnum, I.M., Le Bas, T., Schmidt, V., Keith, G. and Ierodiaconou, D. (2018). Multibeam sonar backscatter data processing. Mar. Geophys. Res. 39, 121–137.

Simons, D.G. and Snellen, M. (2009). A Bayesian approach to seafloor classification using multi-beam echo-sounder backscatter data. Appl. Acoust. 70: 1258–1268.

Snellen, M., Gaida, T.C., Koop, L., Alevizos, E., & Simons, D.G. (2019). Performance of Multibeam Echosounder Backscatter-Based Classification for Monitoring Sediment Distributions Using Multitemporal Large-Scale Ocean Data Sets. *IEEE Journal of Oceanic Engineering,* **44**(1) https://doi.org/10.1109/JOE.2018.2791878.

Van Dijk, T.A.G.P., Van Dalfsen, J.A., Van Lancker, V., Van Overmeeren, R.A., Van Heteren, S. and Doornenbal, P.J. (2012). Benthic habitat variations over tidal ridges, North Sea, The Netherlands. In: Harris, P. and Baker, E. (Eds.): Seafloor Geomorphology as Benthic Habitat; Elsevier: Amsterdam, The Netherlands, pp. 241–249.

Wentworth, C. K. (1922). A Scale of Grade and Class Terms for Clastic Sediments. *The Journal of Geology,* 30(5): 377-392. https://doi.org/10.1086/622910.

8 Appendix 1

Plots of bed classification calculations for MBES beams 37°, 40°, 45°, 51°, 53°, 54°, 56°, 58°, 60°, 61°, 62°, 63° and 64°, and approximations of the corrected backscatter curves with 2 to 8 acoustic classes (Gaussians). In each figure, the first plot displays the number of classes as recommended by the method (red circle on blue line).

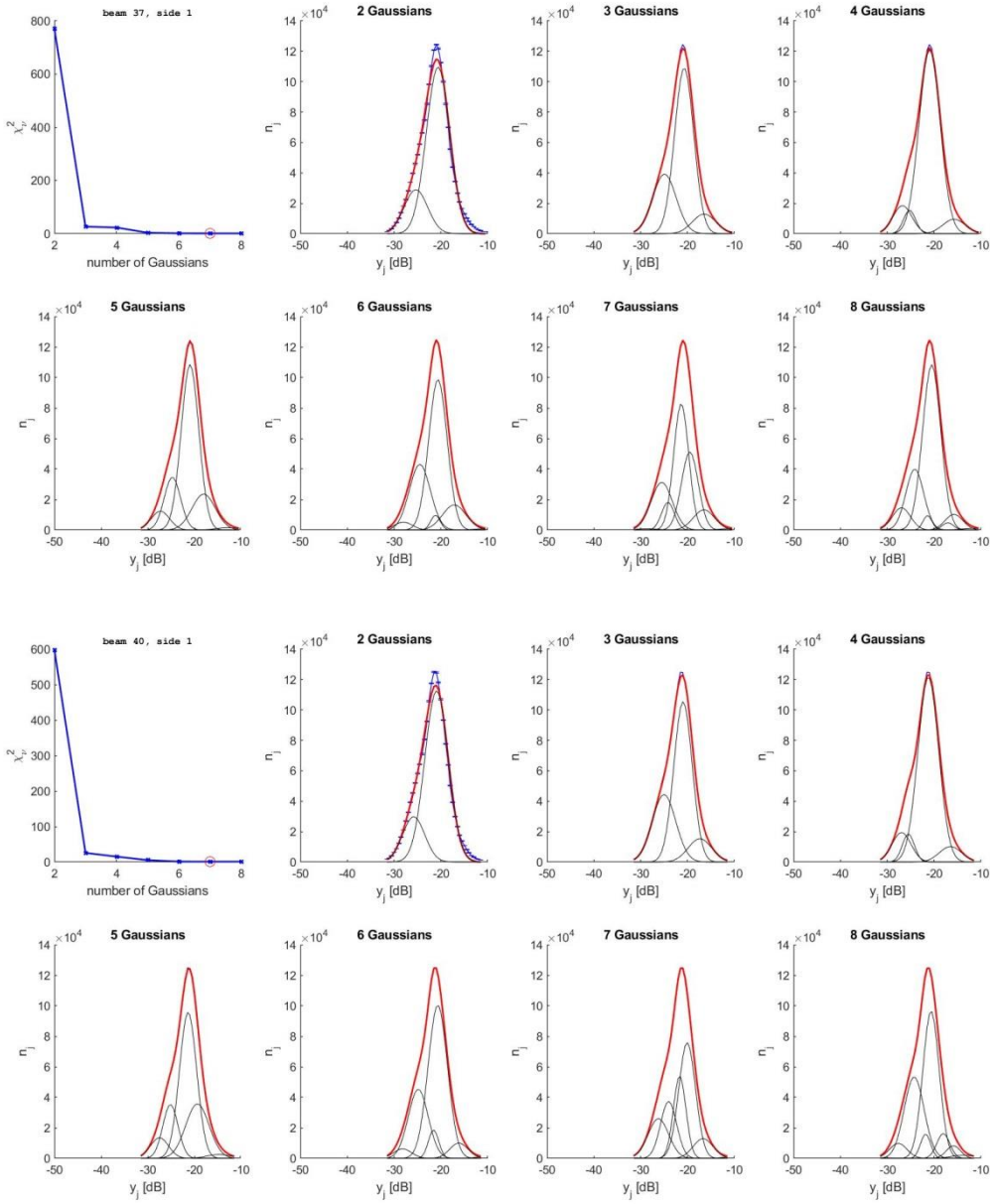

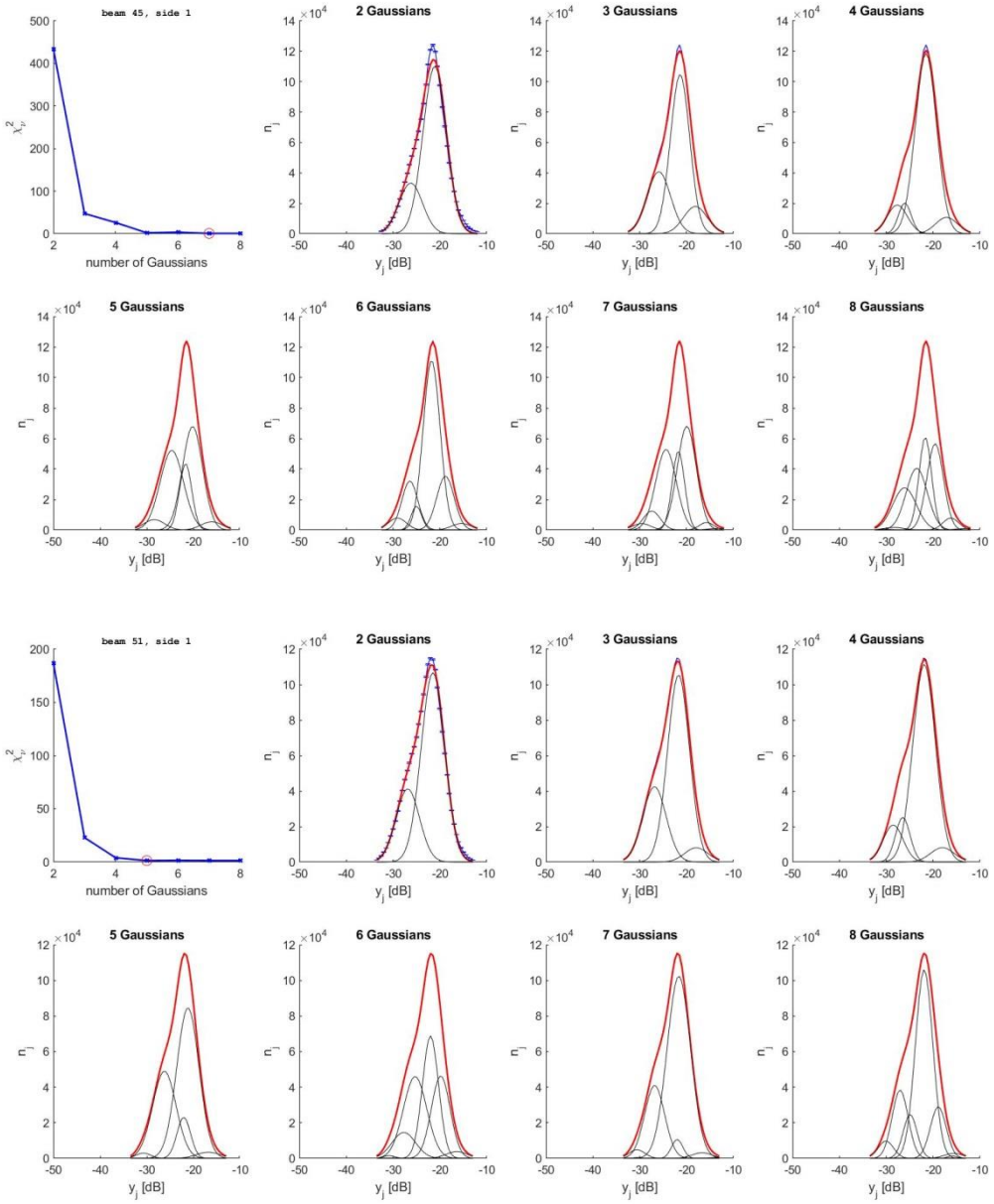
beam 45, side 1
number of Gaussians
2 Gaussians
3 Gaussians
4 Gaussians
5 Gaussians
6 Gaussians
7 Gaussians
8 Gaussians
beam 51, side 1
number of Gaussians
2 Gaussians
3 Gaussians
4 Gaussians
5 Gaussians
6 Gaussians
7 Gaussians
8 Gaussians

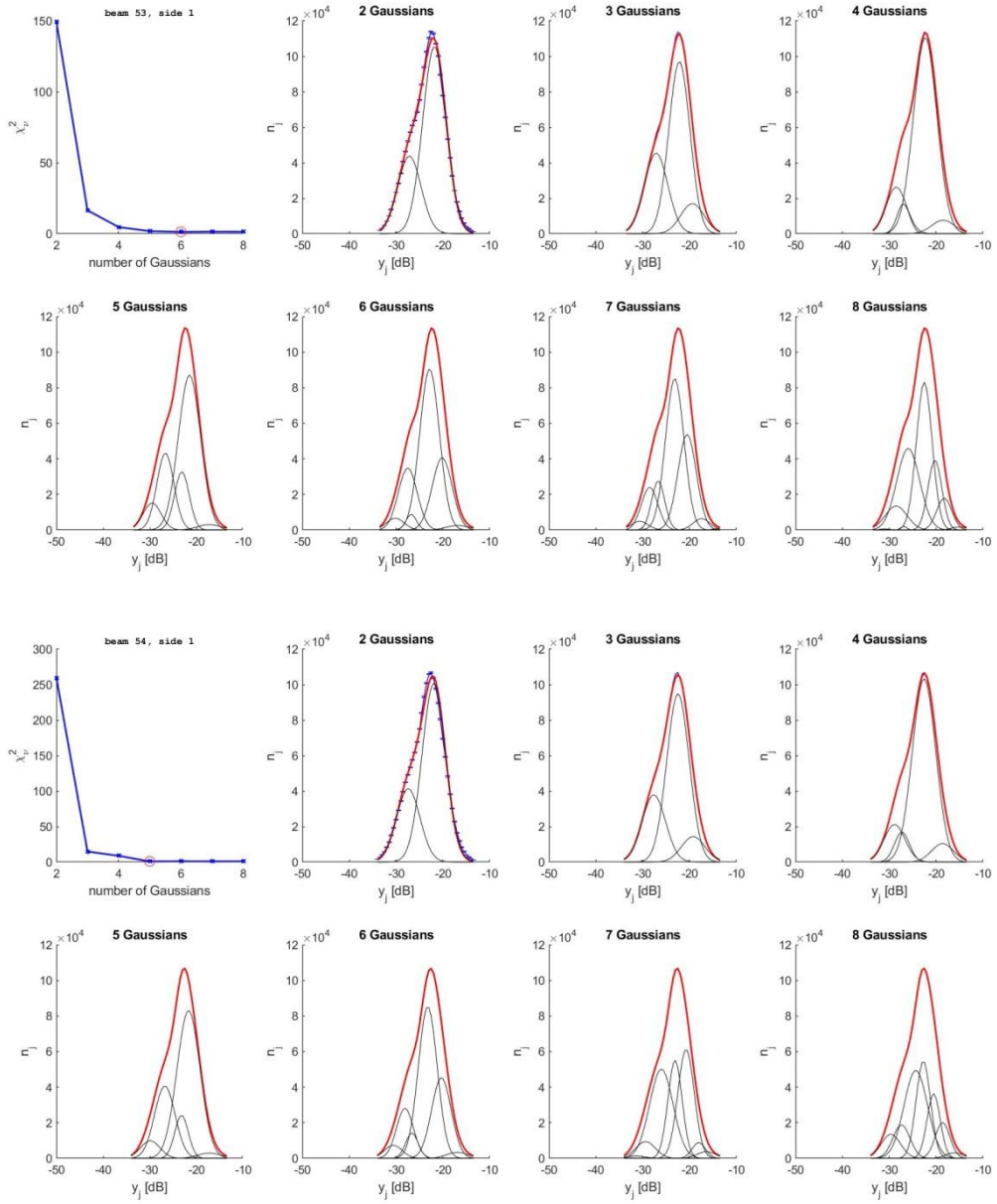
beam 53, side 1
number of Gaussians
2 Gaussians
3 Gaussians
4 Gaussians
5 Gaussians
6 Gaussians
7 Gaussians
8 Gaussians
beam 54, side 1
number of Gaussians
2 Gaussians
3 Gaussians
4 Gaussians
5 Gaussians
6 Gaussians
7 Gaussians
8 Gaussians

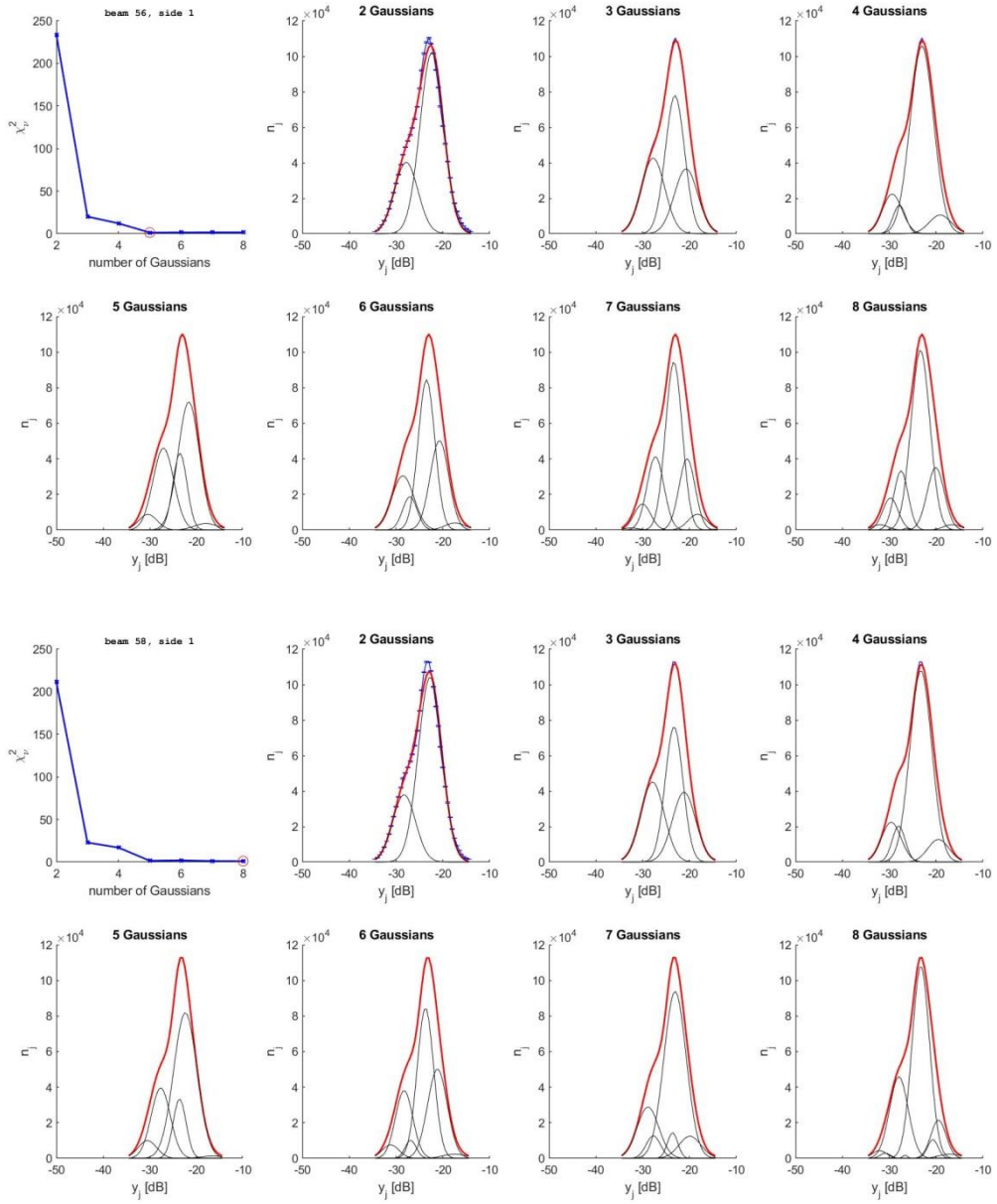
beam 56, side 1
2 Gaussians
3 Gaussians
4 Gaussians
5 Gaussians
6 Gaussians
7 Gaussians
8 Gaussians
number of Gaussians
y_j [dB]
n_j
beam 58, side 1
2 Gaussians
3 Gaussians
4 Gaussians
5 Gaussians
6 Gaussians
7 Gaussians
8 Gaussians
number of Gaussians
y_j [dB]
n_j

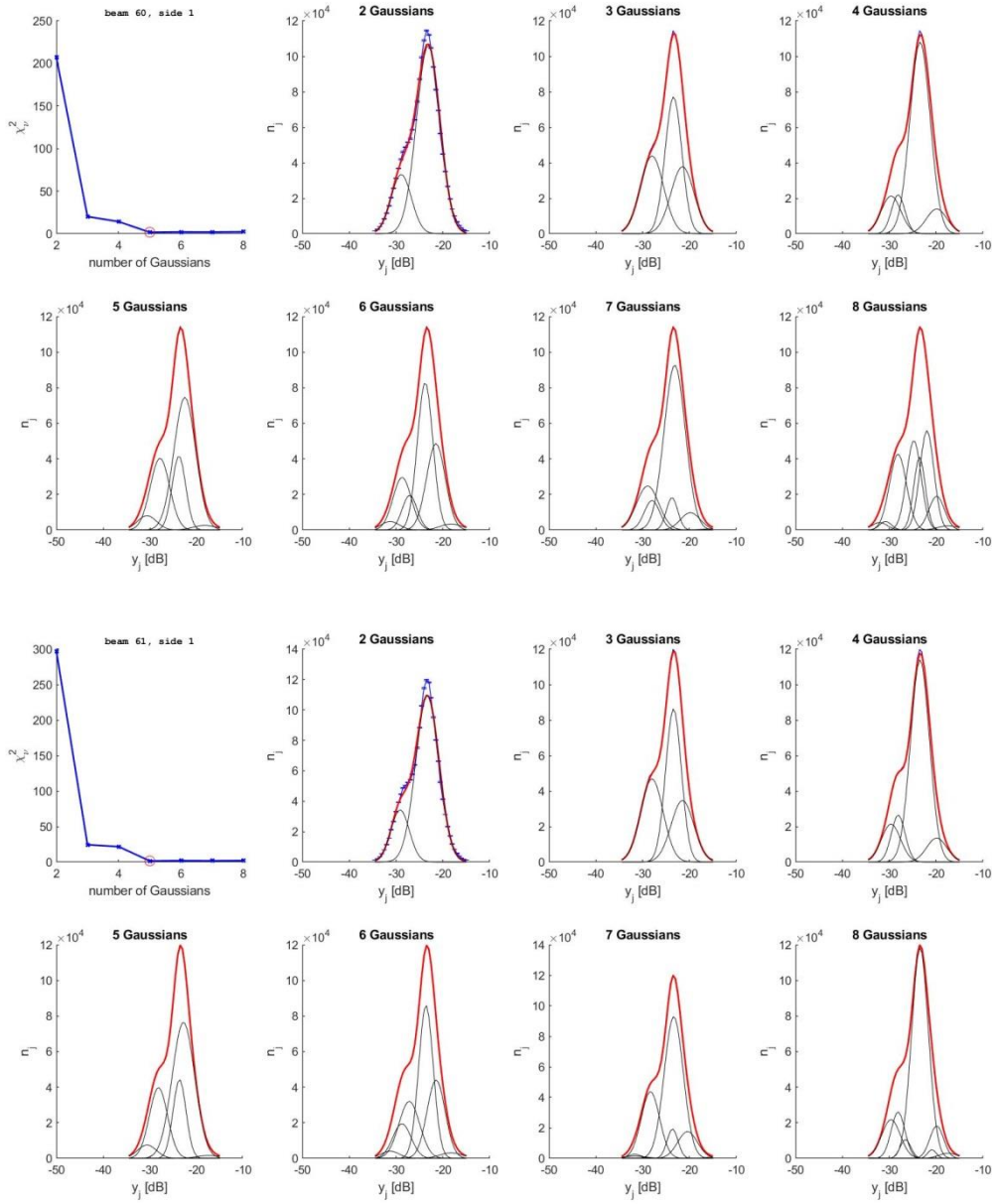
beam 60, side 1
2 Gaussians
3 Gaussians
4 Gaussians
5 Gaussians
6 Gaussians
7 Gaussians
8 Gaussians
number of Gaussians
beam 61, side 1
2 Gaussians
3 Gaussians
4 Gaussians
5 Gaussians
6 Gaussians
7 Gaussians
8 Gaussians
number of Gaussians

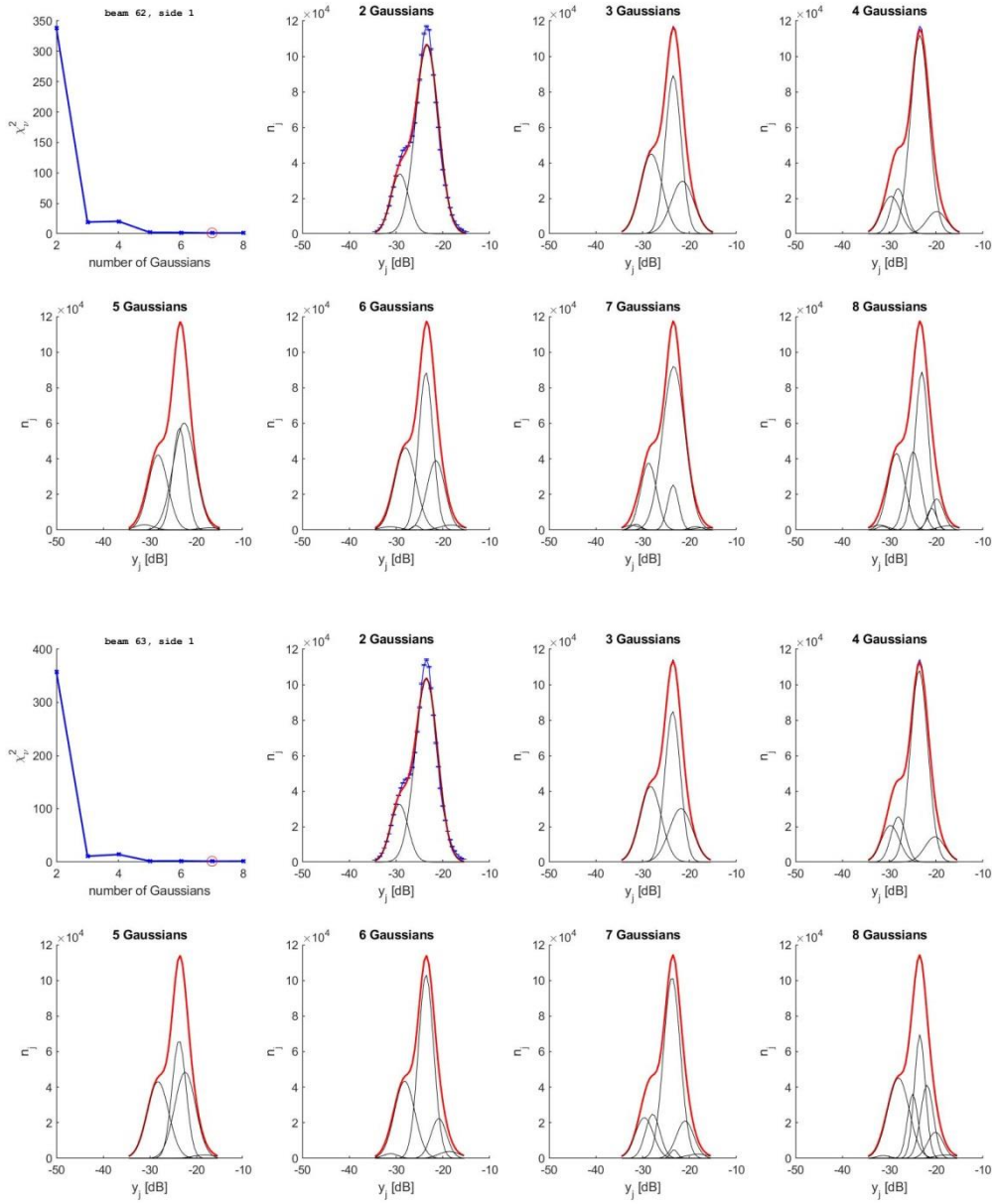
beam 62, side 1
number of Gaussians
2 Gaussians
3 Gaussians
4 Gaussians
5 Gaussians
6 Gaussians
7 Gaussians
8 Gaussians
beam 63, side 1
number of Gaussians
2 Gaussians
3 Gaussians
4 Gaussians
5 Gaussians
6 Gaussians
7 Gaussians
8 Gaussians

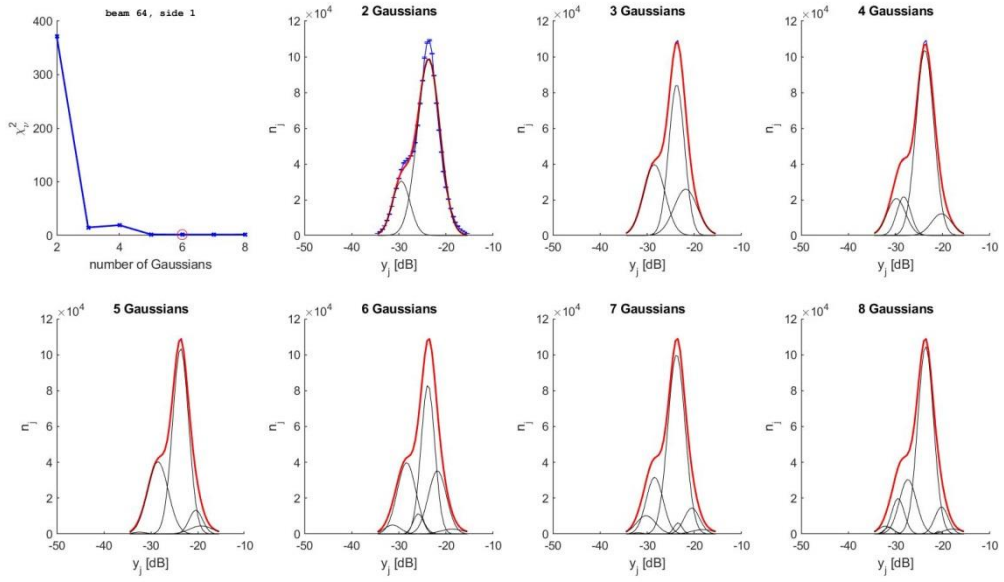
beam 64, side 1
number of Gaussians
2 Gaussians
3 Gaussians
4 Gaussians
5 Gaussians
6 Gaussians
7 Gaussians
8 Gaussians
y_j [dB]
n_j